

Dissolution Patterns Prediction in Carbonate System

Andrei S. Margert

Supervisors: Dr. Denis Voskov
Dr. Sebastien Vincent-Bonnieu



Dissolution Patterns Prediction in Carbonate System

by

Andrei S. Margert

to obtain the degree of Master of Science

at the Delft University of Technology,

to be defended publicly on Wednesday, November 27, 2019 at 15:00.

Student number: 4747909
Project duration: November 12, 2018 – November 27, 2019
Thesis committee: Dr. D. V. Voskov, TU Delft, supervisor
Dr. S. Vincent-Bonnieu, Shell Global Solutions International B.V., co-supervisor
Dr. B. Rossen, TU Delft
Dr. K. H. A. A. Wolf, TU Delft
Dr. J. Snippe, Shell Global Solutions International B.V.
PhD candidate S. de Hoop, TU Delft

An electronic version of this thesis is available at <http://repository.tudelft.nl/>.

Abstract

Acidizing is a widely used technique for intensification of geothermal wells. At certain conditions, acid injection results in a formation of highly conductive channels, e.g. wormholes. The associated rock matrix dissolution is highly nonlinear and may influence the fluid flow as well as rock properties. Wormhole patterns and breakthrough time are mainly controlled by acid strength and injection rate. Due to high complexity and, therefore, high computational cost, existing conventional simulators usually do not include complex chemical reactions or use weak (sequential) coupling of flow with reactive transport. Although the sequential approach is good for various applications, it is limited by the CFL condition and might suffer from poor convergence. In this project, we investigate the wormhole phenomenon to provide a stable fully implicit method (FIM) to numerically solve the reactive flow and transport problem coupled with equilibrium and kinetic reactions associated with the acid injection. The developed framework is aimed to predict a pattern of dissolution as well as wormhole breakthrough time. For an accurate description of species interactions, we directly connect PHREEQC equilibrium computation with FIM framework for kinetic dissolution using the Element Balance approach. This coupling was achieved with an application of a recently introduced Operator-Based Linearization scheme utilized within a Delft Advanced Research Terra Simulator (DARTS).

Acknowledgement

I want to express my deepest gratitude to my supervisors Dr. Denis Voskov and Dr. Sebastien Vincent-Bonnieu for guiding me through this project and their time they dedicated to help me. I would also like to say thanks to my co-supervisor and PhD candidate Stephan de Hoop and Dr. Mark Khait for the help with physical and chemical concepts and implementation of required routines into DARTS. I highly appreciate the experience that Dr. Jeroen Snippe and Dr. Steffen Berg shared with me and their guidance. I am much obliged for Shell's financial support, which allowed me to work on the MSc thesis for a longer time and access valuable proprietary study sources. Special thanks to Dr. Jiakun Gong and Dr. Swej Shah for their help with image processing tools.

I want to thank my family for their support. It all would be impossible without them.

List of Figures

1.1	Simplified THOUGHREACT flow chart from [22]	6
1.2	Fully implicit method flow chart	8
2.1	Resulting binaries for different Gaussian kernel sizes	14
2.2	Final results of CT pre-processing	14
2.3	CT filtering results	15
2.4	Mesh comparison	15
2.5	Mesh resolution control	16
2.6	Core porosity map	16
3.1	Initialization flowchart	22
4.1	Resulting solid saturation in 1D after 10 pore volumes injected	24
4.2	Initial porosity distribution in 2D	25
4.3	2D simulation results	25
4.4	2D model pressure drop (bar)	26
4.5	Solid phase molar fraction	27

List of Tables

4.1	Computer configuration	23
4.2	1D model configuration	23
4.3	2D model configuration	24
4.4	2D simulation performance	26
4.5	2D simulation performance	26
4.6	3D model configuration	27
4.7	3D simulation performance	27

Contents

List of Figures	vii
List of Tables	ix
1 Introduction and Literature	1
1.1 Literature review	2
1.1.1 Chemical reactions	3
1.1.2 Numerical schemes	4
1.1.3 Nonlinear formulations	4
1.1.4 Reactive transport simulations	5
1.2 Element based formulation.	5
1.3 Operator-Based Linearization	8
1.4 Scope of this work	10
1.5 Dissertation outline	10
2 Experimental Data and Processing	11
2.1 Experiment overview	11
2.2 Core characterization.	11
2.2.1 Pre-processing	13
2.3 Results	14
3 Simulation Model	17
3.1 Aqueous model and reduction to elements	17
3.2 PHREEQC modeling	18
3.2.1 Thermodynamic and chemical equilibrium	19
3.2.2 PHREEQC – DARTS coupling.	20
3.3 Kinetic reaction rate	20

3.4	Permeability treatment	21
3.5	Model initialization	21
4	Reactive Transport Simulation Results	23
4.1	Reactive transport in 1D	23
4.2	Reactive transport in 2D	24
4.3	Reactive transport in 3D	26
5	Conclusion and Recommendations for Future Work	29
	Bibliography	31

Introduction and Literature

Reservoir simulation has become an integral part of the industrial applications in subsurface. This tool allows for a wise use of the available assets to achieve the best production efficiency. The development of such modeling capacity is associated with the various fields of study, including applied sciences, numerical and linear algebra, computer science and others. Such diversity is required because of the nonlinear nature of the fluid flow in porous media. Analytical computational methods are not capable of solving such systems of ordinary or partial differential equations (ODE and PDE, respectively) that most of the related physical phenomena are expressed in. Therefore, even a simple cases of fluid flow in porous media are resolved numerically. Besides petroleum industry, reservoir simulation software is used for geothermal and carbon capture and storage (CCS) applications.

Additional complexity is introduced by the subsurface fluid phase behavior, which can co-exist in vapor and liquid phases with the presence of solid phase. Exact partitioning of phase compositions depends on pressure, temperature and mass of each component in the fluid. It is also possible that phase behavior is dependent on chemical reactions. Besides, various components present in the subsurface initially, several recovery techniques involve injection of multi-component mixtures that may interact with either rock or fluid, or both.

These techniques are usually applied in the course of enhanced oil recovery (EOR) activities during secondary production stage or in CO₂ sequestration projects. A variety EOR methods exists nowadays, like injection of foam, surfactants, polymers, acids, CO₂ and many others. Increasing number of components and their interactions result in a system of multiple nonlinear PDE's. In order to provide accurate results, one may increase spacial or temporal resolution. In fact, better accuracy often counterbalanced by increase of computational costs, especially for complex systems. To solve transport problem in porous media with chemical reactions involved, advanced numerical modeling approach is required.

In this work, we focus on modeling of acidizing technique relevant to various subsurface application which involves many chemical reactions as well as multiphase flow. The main goal is to develop a fully implicit reactive transport solver for CO₂ and water co-injection into carbonate reservoir, as of calcite, withing the Delft Advanced Research Terra Simulator (DARTS). The existing lab experiments, investigating of calcite rock acidic treatment, are used to validate the designed approach.

1.1. Literature review

Acidic treatment is a widely used technique to increase rock permeability [9]. This technology was also successfully applied in Berlin [3] and in Las Tres Virgenes [32] Geothermal Fields. Acid injection into carbonate rock at a certain conditions leads to the formation of highly conductive channels, so-called wormholes [29]. The width of these channels may vary from pore size to a several millimeters and in length they can grow up to tens of meters. This effect can be achieved by co-injection of CO₂ and water due to the ability of carbon dioxide to form a weak diprotic acid that dissolves carbonates.

Natural rock dissolution is a highly non-linear process and depends on flow regime and mineral kinetic rates. Nevertheless, dissolution patterns can be described by two characteristic numbers: Damköhler number, the relation of surface reaction rate to mean fluid velocity, and Péclet number, the relation between advective and diffusive transport rates [7, 20, 25, 31, 56, 61]. Five dissolution regimes are distinguished according to [20, 26, 56]: compact dissolution, conical dissolution, one dominant wormhole, ramified wormholes and uniform dissolution. Each one is described in [26] and [20].

- Compact dissolution: in the case of low flow rate the acid is fully consumed at the inlet of the core, resulting in diffusion domination over transport. Therefore instabilities, hence wormholes, cannot develop.
- Conical dissolution: conical shaped wormholes start to develop at slightly higher injection rate although diffusion is still dominant. It happens because some quantity of the acid penetrates a little deeper in the formation.
- One dominant wormhole: at the intermediate flow rates the fluid with dissolved acid starts to penetrate region with higher permeability leading to the formation of one dominant wormhole. Spatial variation of reactant becomes significant.
- Ramified wormholes: when the flow rate is high wormholes start to branch and form ramified structure. The dissolution front spreads over porous domain.
- Uniform dissolution: at the very high flow rates acid solution reaches all possible regions of the domain. The dissolution front spreads over the whole sample. Despite small amount of time for the reaction between acid and rock matrix this regime results in uniform displacement.

Any regime can be achieved by the control over Péclet and Damköhler numbers. Péclet number is controlled by injection flow rate. Damköhler number depends on a particular mineral and acid properties. Hence, control can be done with an acid type and its concentration.

The porous media dissolution has been studied at a different scales. Pore scale investigations [38, 43, 58] provide a better understanding of chemical interactions in porous environment. Still, such description becomes sufficiently complicated due to the size of the model, which rapidly increases with the number of pores involved. There are continuous attempts on pore scale modeling improvements [5, 30, 42] not only for reactive transport problem, but also beyond. More elaborate overview on the pore scale modeling advances and challenges are given in [33]. Darcy scale (REV or continuum) studies [20, 41, 44, 55] are instead focused on development of the solution with practical application potential. They aim not only for accurate physics representation, but also tend to lower a run time.

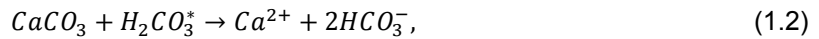
There is also another branch of researches that are focused on implementation of Darcy-Brinkman-Stokes (DBS) equation instead of Darcy law in order to capture physics of the process with higher degree of accuracy. According to a recent study [62] DBS model allows for more detailed description of the flow in cases when porosity of representative elementary

volume (REV) or control volume becomes close to 100%. However, approach is adaptive, since global DBS application introduces significant computational overhead, which is not an option for real-life usage. Indeed, according to comparative study of Darcy and DBS models performed before in [51] results may vary depending on the applied model. Although considerable difference in the shape was observed, though Darcy model constantly demonstrated lower injected pore volumes before the wormhole breakthrough than DBS model, indicating a possibility of correction by upscaling or similar techniques.

There are continuous attempts to use the extended DBS formulation to apply it for the multiphase flow, like [57]. Existent researches in this area are not limited to the given examples and there are a lot more. In this work we attempt to develop a Darcy scale predictive wormhole model based on Darcy law for flow description. DBS implementation is left for later investigations.

1.1.1. Chemical reactions

Carbonates dissolution was extensively studied compared to the other mineral classes. Although first studies of calcite dissolution rate were limited to the influence of pH and degree of undersaturation of aqueous solution, later works [48] put their emphasis on investigation of other influencing factors: activity of H^+ , temperature and CO_2 partial pressure. As suggested by Plummer et al. calcite dissolution can be described by three parallel reactions, obeying different dependencies [12]:



where $H_2CO_3^*$ represents the sum of molecular CO_2 and H_2CO_3 dissolved in aqueous phase.

Beside different calcite dissolution mechanism, there are other important interactions that should be considered. First of all, CO_2 dissolution:



Whereas calcite is almost insoluble in pH – neutral water, presence of dissolved carbon dioxide sufficiently increases its solubility. In the aqueous phase CO_2 and water form carbonic acid, which is weak diprotic acid:



It further dissociates in two stages:



Usually the concentration of HCO_3^- dominates over H_2CO_3 , so more common written form of eq.(1.5) is:



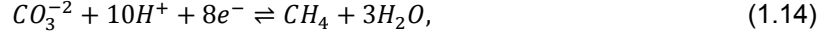
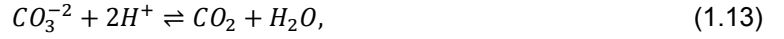
In a small quantities water dissociates too:



For this system to achieve chemical equilibrium it should satisfy the charge balance condition [48]:

$$2Ca^{2+} - HCO_3^- - 2CO_3^{2-} + H^+ - OH^- = 0. \quad (1.10)$$

For all the dissolved components, there are many other chemical interactions that they undergo:



Most of these reactions do not happen intensively relatively to predominant reactions stated earlier and even not all of them are always very likely to occur. Nevertheless, in modeling of chemical reactions, all interactions are taken into account. This will be described in more detail in chapter 3.

1.1.2. Numerical schemes

There are two different numerical schemes to solve coupled flow and transport with chemical reactions: sequential approach (SA) also known as operator splitting (OS) and direct substitution approach (DSA) or global implicit approach (GIA) [21, 23, 72].

OS might be of two types: iterative (SIA) and non-iterative (SNIA). Generally, in OS, transport and reaction equations are treated separately for each time step. First, the new pressure gradient is computed with the flow determining parameters assumed to be constant. Next, the concentrations are updated in every block of discretized space with the obtained phase velocities and compositions. SIA iterates between splitted equations until convergence [19]. SNIA does not [50]. As an example, shortened THOUGHREACT flow chart is given in figure 1.1. According to [71], OS methods are proven to be more efficient. However, later studies report a splitting error due to decoupling transport and chemistry [4, 8], SIA minimizes this effect. In addition, such approach is known to have convergence problems, especially for a large time steps or complex systems [50].

GIA appeared to be more stable and, therefore, preferable for complex systems [21]. But this approach is much harder to implement and it is also more demanding in terms of memory and computational power [72]. GIA makes no approximation in the formulation of the Jacobian matrix and includes all derivatives and the transport and reaction terms are solved simultaneously. This can become a serious limitation in the case of large systems due to species coupling via reactions. The performance of this method is controlled by the efficiency of the Newton-Raphson loop on solving the system of nonlinear equations [49]. However, GIA is reported to be more stable than both SIA and SNIA [21, 59]. Although, this approach is difficult to implement and it requires more resources for computations, GIA can perform a large time steps without stability problems.

1.1.3. Nonlinear formulations

Nonlinearity of the governing equations in the area of reservoir simulations is usually resolved by Newton-Raphson method:

$$\mathbf{J}(\boldsymbol{\gamma}^{\mathbf{k}})(\boldsymbol{\gamma}^{\mathbf{k}+1} - \boldsymbol{\gamma}^{\mathbf{k}}) = -\mathbf{r}(\boldsymbol{\gamma}^{\mathbf{k}}), \quad (1.17)$$

where \mathbf{J} stands for the Jacobian matrix with respect to the primary unknowns, $\boldsymbol{\gamma}$ is the set of primary unknowns, \mathbf{k} is the nonlinear iteration and \mathbf{r} is the residual. Once residual is dropped below the predefined tolerance, the values of the primary unknowns are updated.

Depending on a set of primary equations different nonlinear formulations can be applied for a reactive-composition flow and transport problem. There are mainly two approaches

used in the reservoir engineering community: natural formulation [14] and molar formulation [1, 11].

For the natural formulation primary unknowns are chosen to be pressure, saturations and phase compositions. Phase behavior is not required to be evaluated for each Newton iteration, but only when it converges. Drawback here is that number of phases present in a control volume. Molar formulation defines the primary unknowns as pressure and component molar fractions. Here each Newton iteration solves flash for secondary unknowns (phase saturations and compositions). Therefore each iteration becomes computationally expensive. More evolved overview of these techniques can be found in [67].

For this study we use molar formulation. Such decision is reasoned by advanced algebraic technique that helps to resolve the computational overhead of the chosen formulation. It is described in detail in chapter 1.3.

1.1.4. Reactive transport simulations

In the last years, the reactive transport simulation software has been developed remarkably [59]. Various solutions are present nowadays. All of them can be divided into two major groups according to the development community: groundwater and reservoir engineering. Brief description of some simulators is given in this section.

Some examples of reactive flow and transport simulators from the groundwater community contributors are THOUGHREACT [70], PFLOTTRAN [40] and Crunch-flow [60]. THOUGHREACT is a thermal multi-component reactive transport simulator, developed at Berkeley National Laboratory. It utilizes sequential iterative approach and also capable of multiphase flow. PFLOTTRAN utilizes global implicit approach and treats multi-component multiphase flow. Crunch-flow is quite similar to THOUGHREACT but it does not treat multiple phases.

In the reservoir engineering community, reactive flow and transport software includes the following simulators: GPRS [22], UTCHEM [63] and GEM [15]. GPRS and GEM are fully implicit simulators with kinetic and equilibrium reactions included. Both based on generalized equation of state (EOS). UTCHEM is a sequential iterative simulator with pressure treated implicitly. All of these simulators are three-dimensional.

1.2. Element based formulation

To reduce the level of model complexity, an element based formulation of the governing equation can be utilized as it is described in the previous works [34, 39]. The conservation of species:

$$\frac{\partial n_c}{\partial t} + l_c + q_c = \sum_{k=1}^K v_{ck} r_k + \sum_{q=1}^Q v_{cq} r_q, \quad (1.18)$$

where n_c – overall mass of component, l_c – total flux of a component c , v_{ck} – stoichiometric coefficient of a component c in kinetic reaction k , v_{cq} – stoichiometric coefficient of a component c in equilibrium reaction q , r_k – rate of a kinetic reaction k and r_q – rate of an equilibrium reaction q . Written in a vector form, eq.(1.18) becomes:

$$\frac{\partial \mathbf{n}}{\partial t} + \mathbf{l} + \mathbf{q} = \mathbf{V} \mathbf{r}, \quad (1.19)$$

where $\mathbf{n} = (n_1, \dots, n_c)^T$, $\mathbf{l} = (l_1, \dots, l_c)^T$, \mathbf{V} is the stoichiometric matrix in a reaction and $\mathbf{r} = (r_1, \dots, r_{q+k})^T$. Further reduction to elements requires introduction of stoichiometry and equilibrium rate annihilation matrices as suggested in [22, 23]. Canonically, stoichiometry matrix (\mathbf{S}) is defined in terms of species and elements.

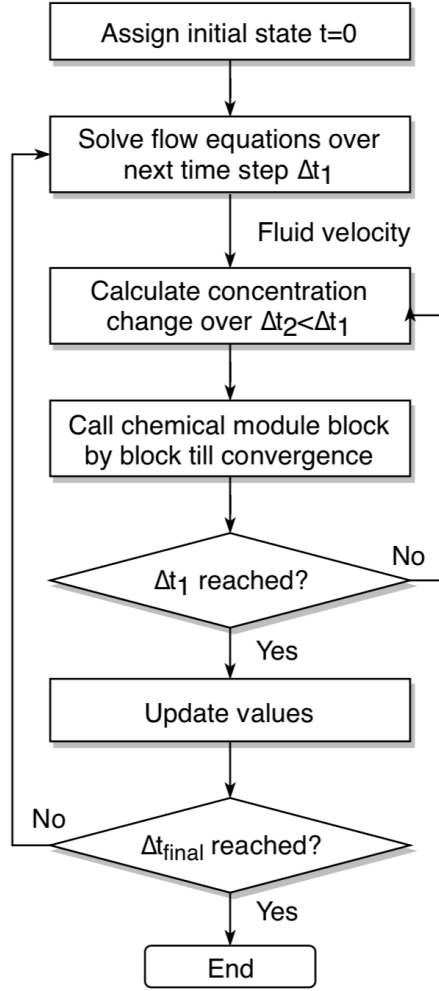


Figure 1.1: Simplified THOUGHREACT flow chart from [22]

Species are non-unique components of reactions that can be uniquely composed with elements. From now on species are called components in this work. The general form of \mathbf{S} matrix is given as:

$$\mathbf{S}_{C \times R} = \left[\begin{array}{c|c} \mathbf{Q}_{Q \times K} & -\mathbf{I}_{1, Q \times Q} \\ \hline -\mathbf{I}_{2, K \times K} & \mathbf{S}_{3, K \times Q} \\ \hline \mathbf{S}_{1, (C-R) \times K} & \mathbf{S}_{2, (C-R) \times Q} \end{array} \right] \quad (1.20)$$

where R is the total number of reactions, Q is the number of equilibrium reactions, K is the number of kinetic reactions and C is the number of components (species). Left column corresponds to kinetic reactions and right to equilibrium. Horizontal dashed line separates species (top) and elements (bottom). Rate annihilation matrix is defined as follows:

$$\mathbf{E}_{(E+K) \times C} = \begin{bmatrix} \mathbf{E}_{1, (E \times C)} \\ \mathbf{E}_{2, (K \times C)} \end{bmatrix}, \quad (1.21)$$

where

$$\mathbf{E}_{1(E \times C)} = \begin{bmatrix} e_{11} & e_{12} & \dots & e_{1C} \\ e_{21} & e_{22} & \dots & e_{2C} \\ \dots & \dots & \ddots & \dots \\ e_{E1} & e_{E2} & \dots & e_{EC} \end{bmatrix}, \quad (1.22)$$

and

$$\mathbf{E}_{2(K \times C)} = [-\mathbf{S}_{1, K \times Q} \quad -\mathbf{I}_{2, K \times K} \quad \mathbf{0}_{K \times (C-R)}]. \quad (1.23)$$

Here \mathbf{E} stands for elements.

Columns of \mathbf{E} matrix represent components, that are involved in a chemical model and rows represent elements. There are an important conditions that \mathbf{S} and \mathbf{E} matrices should satisfy. The elements should be chosen such that rows of \mathbf{E} matrix are linearly independent, and its set of vectors forms a vector space of the dimension n_e . This implies, that there are no redundant (linearly dependent) elements. Mass balance for all reactions lead to:

$$\mathbf{E} \times \mathbf{S} = \mathbf{0}_{n_e \times n_r}. \quad (1.24)$$

From eq.(1.24), it follows that \mathbf{S} matrix must belong to the null space of \mathbf{E} . This is crucial requirement, because \mathbf{S} matrix must represent a set of linearly independent chemical reactions.

Eq.(1.19) now can be transformed into:

$$\frac{\partial (\mathbf{E}\mathbf{n})}{\partial t} + \mathbf{E}\mathbf{l} = \mathbf{E}\mathbf{S}\mathbf{r} = \begin{bmatrix} \mathbf{E}_1 \mathbf{S}\mathbf{r} \\ \mathbf{E}_2 \mathbf{S}\mathbf{r} \end{bmatrix} = \begin{bmatrix} 0 \\ \mathbf{r}_k \end{bmatrix}. \quad (1.25)$$

From the definition, rate annihilation matrix \mathbf{E} eliminates equilibrium reaction rates. It follows from the law of mass action:

$$Q_q - K_q = \prod_{c=1}^C \alpha_c^{v_{cq}} - K_q = 0, \quad (1.26)$$

where Q_q – activity product of reaction q , K_q – equilibrium constant for reaction q and α_c – activity of component c . This means that equilibrium reactions reach an equilibrium state immediately and depend only on the amount of reactants and products in a particular reaction.

To rewrite an eq.(1.19) in terms of elements, we define overall element composition, \mathbf{z}^E , as:

$$\mathbf{z}^E = \left(\frac{\rho_T}{\rho_T^E} \mathbf{E} \right) \mathbf{z} = \frac{\sum_{c=1}^C e_{ec} z_c}{\sum_{c=1}^C \sum_{e=1}^E e_{ec} z_c}, \quad (1.27)$$

where total component and elements densities are:

$$\rho_T = \sum_{p=1}^P \rho_p S_p = \frac{1}{\sum_{p=1}^P \frac{v_p}{\rho_p}}, \quad (1.28)$$

$$\rho_T^E = \sum_{p=1}^P \left(\rho_p S_p \sum_{c=1}^C \sum_{e=1}^E e_{ec} x_{cp} \right) = \frac{\sum_{c=1}^C \sum_{e=1}^E e_{ec} z_c}{\sum_{p=1}^P \frac{v_p}{\rho_p}}. \quad (1.29)$$

Therefore, eq.(1.25) for equilibrium reactions becomes:

$$\frac{\partial \phi \rho_T^E \mathbf{z}^E}{\partial t} + \mathbf{E}\mathbf{l} = 0, \quad (1.30)$$

and for kinetic reactions it is:

$$\frac{\partial \mathbf{E}_{K \times C} \mathbf{n}_{C \times 1}}{\partial t} + \mathbf{E}_{K \times C} \mathbf{l}_{C \times 1} = \mathbf{r}_k. \quad (1.31)$$

In this work, we study isothermal system and implement molar based formulation, therefore the set of unknowns is:

$$\gamma = (P, z_e, v_p, x_{cp}). \quad (1.32)$$

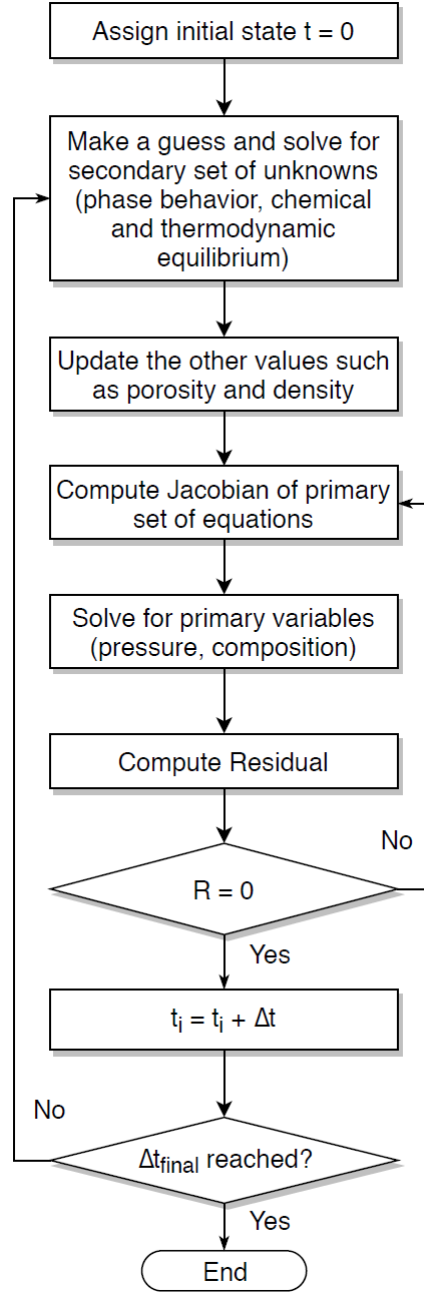


Figure 1.2: Fully implicit method flow chart

1.3. Operator-Based Linearization

In this work, we supplement Newton-Raphson technique with a recently developed fully implicit Operator-Based Linearization (OBL) approach proposed in [66] (OBL flow chart is given in figure 1.2). In this approach, conservation equations are parameterized by division of entities into two groups: space and state dependent. Thus state of the system can be evaluated by a multi-linear interpolation of formulated operators. The following equation is utilized in this study:

$$\frac{\partial}{\partial t} (\phi^T \rho_t z_c) + \nabla \cdot \left(\sum_{j=1}^{n_p} (x_{cj} \rho_j \mathbf{u}_j - \phi^T S_j \rho_j D_{cj} \nabla x_{cj}) \right) = \sum_{k=1}^{n_k} v_{ck} r_k, \quad (1.33)$$

where ϕ^T – total porosity, ρ_t – total density, ρ_j – density of phase j, x_{cj} – mole fraction of component c in phase j, \mathbf{u}_j – Darcy velocity of phase j, S_j – saturation of phase j and D_{cj} – diffusion coefficient of component c in phase j. We define the total porosity as:

$$\phi^T = \frac{1 - S_{solid}}{\phi^f}, \quad (1.34)$$

where ϕ^f – fluid porosity, e.g. pore space. Hence total porosity is the volume fraction of the reactive solid phase and fluid. Since it is assumed that the core is 100% calcite, the total porosity is 1. Darcy velocity is given as:

$$\mathbf{u}_j = -\mathbf{K} \frac{k_{rj}}{\mu_j} (\nabla p - \rho_j g \nabla d), \quad (1.35)$$

where \mathbf{K} – permeability tensor, k_{rj} – relative permeability of phase j, μ_j – dynamic viscosity of phase j and d – depth. Gravity is neglected for simplicity. After finite volume discretization eq.(1.33) becomes:

$$\begin{aligned} V \phi^T \rho^T z_c - (V \phi^T \rho^T z_c)^n - \Delta t \sum_{l \in L} \sum_{j \in n_p} (x_{cj} \rho_j \lambda_j \Gamma^{max} T^M)^l (p - p^l) \\ - \Delta t \sum_{l \in L} \sum_{j \in n_p} (\phi^T S_j \rho_j D_{cj} \Gamma^{diff})^l (x_{cj} - x_{cj}^l) - \Delta t V \sum_{k=1}^{n_k} v_{ck} r_k = 0. \end{aligned} \quad (1.36)$$

And rewritten in operator form, the conservation equations become:

$$a(\xi)(\alpha_c(\omega) - \alpha_c(\omega_n)) + \sum_l (b(\xi, \omega) \beta_c(\omega) + d(\xi, \omega) \delta_c(\omega)) - c(\xi) \gamma_c(\omega) = 0, \quad (1.37)$$

where ω indicates a state dependent and x_i indicates space dependent operators (or multipliers).

- State dependent variables (ω),
 - $k_{rj}(\omega)$ - relative permeability of phase j,
 - $\rho_j(\omega)$ - density of phase j,
 - $S_j(\omega)$ - saturation of phase j,
 - $x_{cj}(\omega)$ - mole fraction of component c in phase j,
 - $\mu_j(\omega)$ - viscosity of phase j.
- Space dependent variables (ξ)
 - $\phi(\xi)$ - porosity.

The operators and their multipliers are defined as:

- $\alpha_c(\omega) = (1 + c_r(p - p_{ref})) \sum_j x_{cj} \rho_j S_j$,
- $\beta_c(\omega) = \sum_j T^M x_{cj}^l \rho_j^l \frac{k_{rj}^l}{\mu_j^l} (p - p^l)$,
- $\gamma_c(\omega) = \sum_k v_{ck} r_k$,
- $\delta_c(\omega) = (1 + c_r(p - p_{ref})) \sum_j \rho_j S_j D_{cj} (x_{cj} - x_{cj}^l)$,

- $a(\xi) = V(\xi)\phi_0(\xi)$,
- $b(\xi, \omega) = \Delta t \Gamma^{l,max}(\xi)$,
- $c(\xi) = \Delta t V(\xi)$,
- $d(\xi, \omega) = \Delta t \Gamma^{diff}(\xi)\phi_0(\xi)$.

In such description operators α , β , γ and δ are state dependent. Their values can be determined for the particular nodes in pressure-composition space, i.e. parameterized as mentioned before. Calculated values of those operators are stored in a special tables and the continuous values are obtained in the course of simulation by interpolation between the nearest known points. It allows for less computations and, hence, improves performance of a simulation. Accuracy is controlled by the amount of nodes where operators are initially calculated.

Further improvement of OBL is proposed by [36] where operator values are calculated adaptively in the course of simulation. Therefore, computationally expensive phase behavior is only evaluated when needed, allowing for even lower simulation run time. This approach is called adaptive OBL. It is applied in Delft Advanced Research Terra Simulator (DARTS) along with advanced computational techniques used in traditional reservoir simulators.

1.4. Scope of this work

In this work we attempt to develop a fully implicit framework for single and two phase reactive transport for CO₂-water mixture in carbonate rock. Linearization is done with OBL and system of equations for secondary unknowns is solved with PHREEQC. After the framework is established and tested, it is implicated in the DARTS framework.

1.5. Dissertation outline

In Chapter 1, a short literature review of the related researches is provided together with description of the chemistry associated with the wormholing phenomenon. Main numerical approaches for solving reactive flow and transport problem and their realizations in different software are also discussed.

In Chapter 2, we describe the main aspect of experimental investigation of the wormholing phenomenon followed by brief overview of the μ CT technology capabilities in the scope of core characterization. The key ideas applied for core properties evaluation and results conclude the chapter.

In Chapter 3, detailed discussion of the applied approach is given. Chemical model and OBL formulation for a particular problem are described along with the assumptions. There are also some details mentioned regarding PHREEQC – DARTS coupling and particular utilization of PHREEQC in this study.

In Chapter 4, we provide the results of numerical experiment. Validation is performed using experimental results.

In Chapter 5, we provide a general concluding remarks of this study: the results are analyzed and possible future improvements are discussed.

2

Experimental Data and Processing

2.1. Experiment overview

The coreflood experiment [53] is studied in this work. Three types of injection are performed: single phase carbonated water injection, two phase water and CO₂ injection and water alternating gas (WAG) injection. All experiments are conducted at constant temperature. Worm-hole breakthrough time is recorded for each investigation. In the course of the experiments, computed tomography (CT) of the core is performed. In this chapter we describe the procedure of core characterization and porosity map construction. We refer to the [54] for detailed description of the experiment and numerical computation regarding that study.

2.2. Core characterization

For results validation purposes, the experimental porous material needs to be described and further used as the porous domain in simulation. Characterization is performed with the simple Python code developed to process a CT scans and interpret obtained information to provide the porosity data.

Computed Tomography (also known as CT or μ CT when applied for core imaging) is a non-destructive imaging technique, with special emphasis on medical applications. Radiographic images of the object at different angles can be processed with filter back projection, which provides 2D slices of the core absorbing materials along the length. With the further processing of consecutive slices, a full 3D reconstruction may be done. Although, image processing is a complex study and not in the scope of this work, we make an attempt to perform a simple analysis of the available information.

The importance of μ CT for visualizing internal object structure is hard to overestimate. Tomographic techniques were widely applied in various studies, in particular, for mobility control in CO₂-enhanced oil recovery [68, 69], for three phase flow [64], for sandstone transport properties computations [2] and fracture geometry quantification [17]. However, conventional μ CT technique has several drawbacks. One is related to the fact that 3D resolution is directly proportional to the size of the X-ray detector and inversely proportional to the size of the sample. Another problem is related to the compromise between power and noise: the increase in power increases the size of minimum attainable X-ray spot size but reduces the noise [18].

Due to the relatively low image resolution, distinguishing between void and rock regions is impossible, hence approach proposed in [37] is not applicable in this case. Therefore, it was decided to determine core porosity using the following equation [52]:

$$\phi = \frac{CT_{brine} - CT_{air}}{CT_w - CT_a}, \quad (2.1)$$

where, CT_{brine} – CT attenuation of fully brine saturated core; CT_{air} – CT attenuation of dry core; CT_w and CT_a – CT attenuation of water and air, respectively. Such correlation is applied for every Region Of Interest (ROI) in the CT image. ROI's are determined as a 2D areas on each CT slice. In order to utilize this approach, Fiji [24] software is used for image processing (filtering and values evaluation). We discuss Fiji's functionality and exact usage later in this chapter. Once $CT_{brine} - CT_{air}$ images are obtained, further processing is performed through the following stages:

- image filtering,
- regions of Interest (ROIs) definition, and
- porosity per ROI value evaluation.

Given that CT images are subject to noise, filtering is necessary. Extensive noise types description can be found in [28]. Here we are dealing mainly with random noise, which appears as fluctuations of image density unpredictably varying from slice to slice, and artifact noise, which is present as predictable and identifiable patterns, like streak artifacts. Two types of filters are subsequently utilized: Kalman stack filtering and Gaussian blur. Kalman filter is a set of linear equations that are applied within so-called self-learning algorithm that takes into account past and current state of the system [73] (in case of CT, neighboring slices). Since the quality of filtering increases as it proceeds, different running schemes were tested. Gaussian blur, similarly to mean filter, blurs the image. It lead to noise elimination and lose of details. This technique is used in order to eliminate residual noise and sharp edges that are left after Kalman filtering. Detail lose is not critical because pore scale information is not of great importance for the purpose of Darcy scale modeling. For further processing ROIs have to be introduced. Gmsh software package [27] is applied for this task. CT post-processing is accomplished with Fiji [24].

Post-processing with Fiji

Fiji (Fiji Is Just ImageJ) [24] is a Java image processing and analysis program. It can calculate area and pixel value statistics of user-defined selections. It can measure distances and angles and can create density histograms and line profile plots. It supports standard image processing functions such as contrast manipulation, sharpening, smoothing, edge detection and median filtering. ImageJ was designed with an open architecture that provides extensibility via Java plugins. Custom acquisition, analysis and processing plugins can be developed using ImageJ's built in editor and Java compiler. User-written plugins make it possible to solve almost any image processing or analysis problem. One of the custom plugins included in Fiji distribution of ImageJ is Kalman stack filter, used in this study.

Gmsh

Gmsh [27] is a free 3D finite element mesh generator with a built-in CAD engine and post-processor. Its design goal is to provide a fast, light and user-friendly meshing tool with parametric input and advanced visualization capabilities. Gmsh is built around four modules: geometry, mesh, solver and post-processing. In the scope of this work, Gmsh software

package is used to introduce unstructured grid representing ROI's on each CT slice. With further processing in Fiji and Python packages, obtained values are transformed into a 3D continuous model of a core.

2.2.1. Pre-processing

Before filtering and introducing ROI's to the CT images some preparation procedures are required:

- erase background,
- locate core contour, and
- configure a geometry for further meshing.

These tasks fall in the computer vision area. OpenCV library for Python [6] is used to pre-process the CT data. As a result of pre-processing, we obtain CT stack without a background as well as core contour that is required for later meshing.

It was decided to construct a binary mask that would have zero values corresponding to background and ones corresponding to the core. Mask construction consists of 2 main steps: blur the image and convert grey scale image to binary. The first step is blurring. Gaussian blur algorithm is utilized. Fitting parameters are width and height of Gaussian kernel, and standard deviation along the x-axis (σ). That is to say, height and width of Gaussian kernel defines the number of neighbors that are involved in smoothing for a particular pixel and standard deviation defines the contributing weights of those neighbors. By varying these parameters, it must be achieved that there are no other big bright areas (where the pixel values are ones) other than core. It is also important to make the core area as clean as possible (without black spots, zeros). Otherwise, core contour might occur to be not identifiable among other features detected by the algorithm. At the same time, blurring should not be too strong because it would lead to incorrect contour evaluation and loss of valuable information.

Next step is to convert blurred grey scale image to binary. Fitting parameter here is a threshold that determines whether a particular pixel is black or white. Resulting binary images for different Gaussian kernel heights and widths are given in figure 2.1.

Using such framework, binary images are obtained for every slice in CT stack except for some slices at the ends of the core, because core is not well pronounced there. Since the core is not perfectly aligned in the jacket, its image may not be always at the same location throughout stack. To correct for this shift, we multiply all binary images which provides an intersection of core area among the whole stack. Although, this may lead to loss of small near-edge regions, it helps to exclude non-core information more precisely, accounting for a parts of the core where glue has penetrated it.

Obtained mask is applied to the CT stack simply by multiplication of each slice in a stack by a mask (2.2). Contour is evaluated using mask as a sharp representation of a core position in the CT. It is represented as a collection of dots, described by two numbers: x and y coordinate in the image. Considering specifics of the Gmsh software, the length of an element produced depends on the distance between adjacent dots of the contour. Therefore, we erase some points in order to control the mesh resolution.

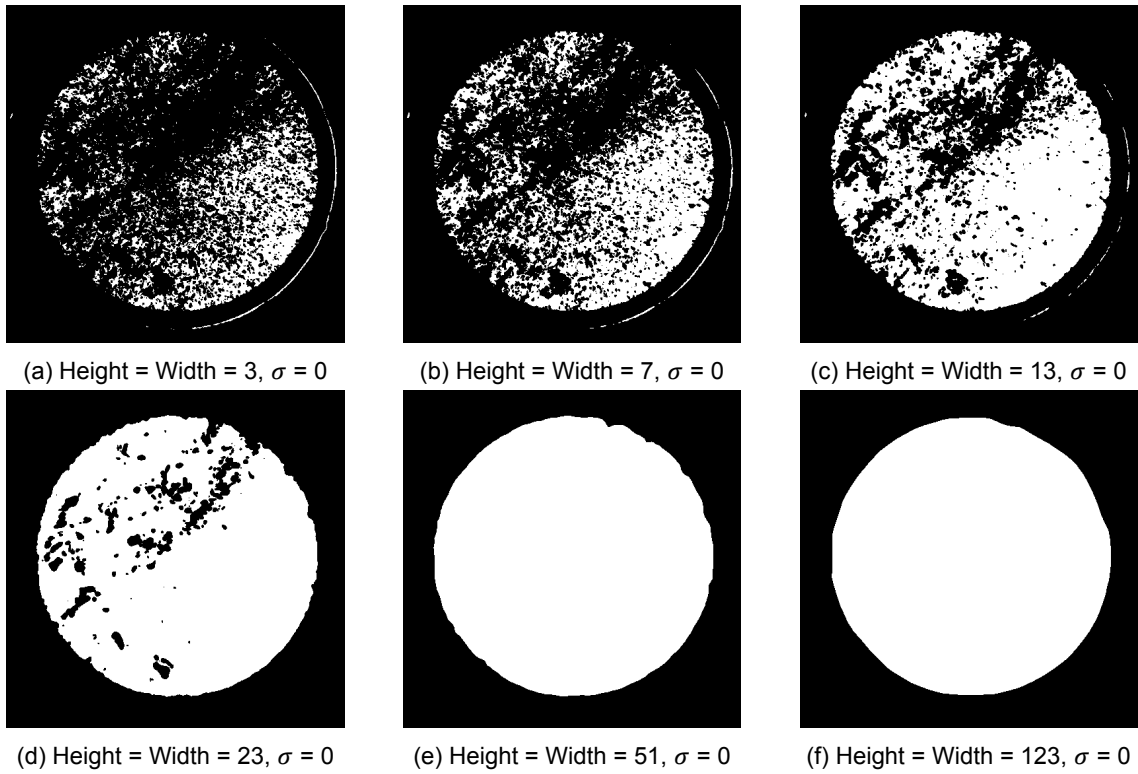


Figure 2.1: Resulting binaries for different Gaussian kernel sizes

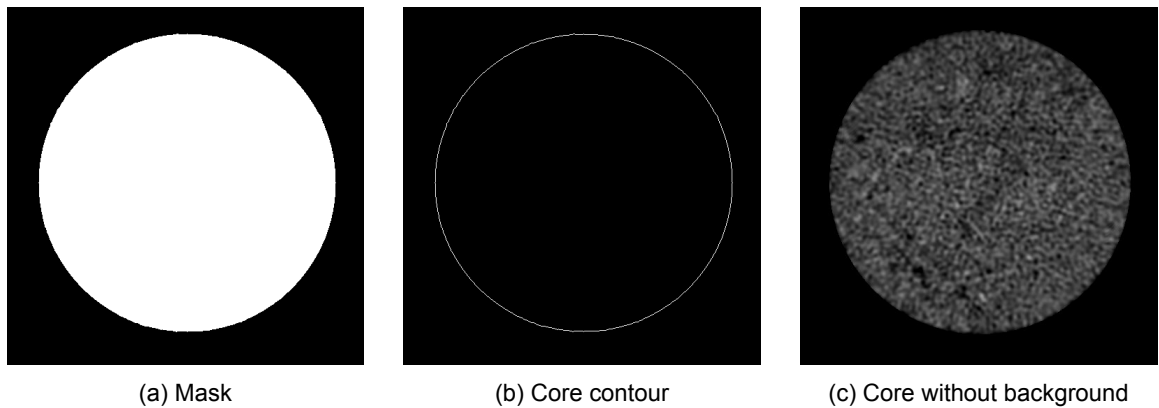


Figure 2.2: Final results of CT pre-processing

2.3. Results

As it was stated earlier, Kalman stack filter together with Gaussian blur are applied to get rid of the noise. The results are given in the figure 2.3.

With a simple Python program and Gmsh software, being compatible with scripting languages, 2D unstructured mesh is built and introduced to Fiji as shown in figure 2.4. We also demonstrate mesh resolution control results in figure 2.5. Important to notice, due to the Fiji inability to accept decimal coordinates of mesh nodes those coordinates were rounded to integer values. As soon as mesh configuration is translated to Fiji, Gaussian blur is applied to eliminate sharp edges and decrease noise influence on final readings. Finally, mean grey scale value is evaluated. Then, using eq.(2.1) core porosity map is constructed (figure 2.6). The values of porosity for 3D porosity map are calculated as a simple average between

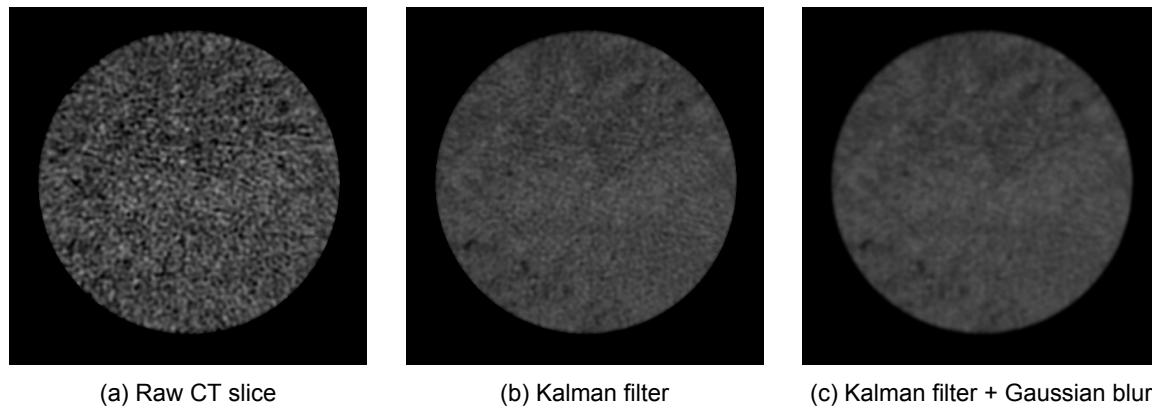


Figure 2.3: CT filtering results

corresponding ROI's at the adjacent slices.

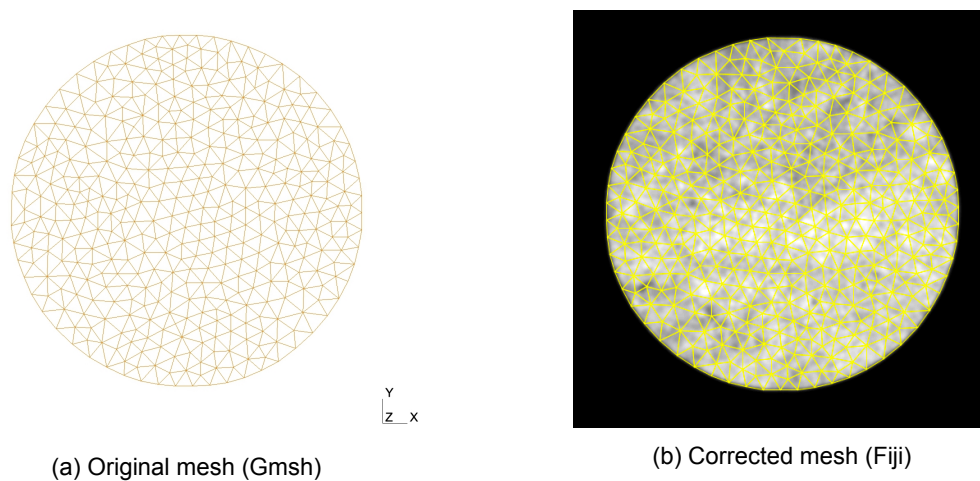


Figure 2.4: Mesh comparison

With the described approach we have managed to obtain a semi-unstructured grid over a 3D domain. The porosity data restored from CT scan is in good agreement with the reported values for this rock (name and resources are not mentioned for confidentiality reasons). Developed approach can be applied for any kind of core CT with the minor adjustments of the algorithm parameters. Filtering procedure is also adjustable, however the intensity of filtering can be only set correctly with the validation of the geologist that is familiar with a particular rock type.

Fiji software can be substituted with the computational geometry packages, such as Pillow or Scipy [65]. It would result in more robust and adjustable algorithm and possibly smaller run time. As a future work, Gmsh is also replaceable, for example SfePy [13]. Once applied the resulting project would have less high level dependencies and more potential for further development and maintenance.

More accurate modeling of a core with a CT as input can be possibly done with more resolved data, where unambiguous distinguishing between pore and rock regions is possible. We refer to the approach described in [37]. Such framework allows for better capturing of a spatial correlation of the porosity.

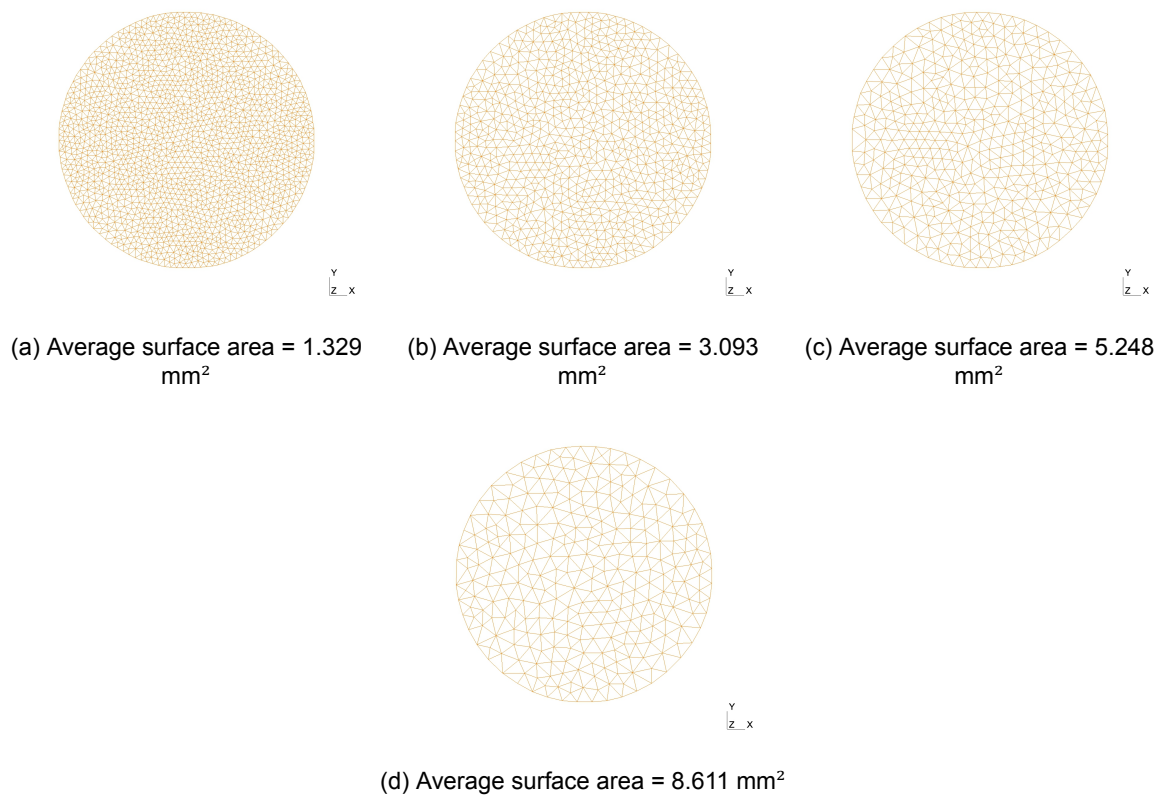


Figure 2.5: Mesh resolution control

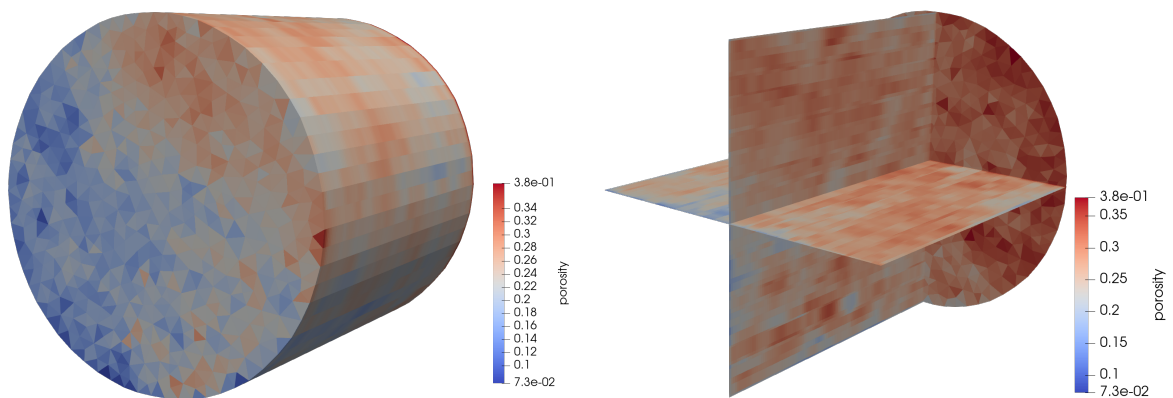


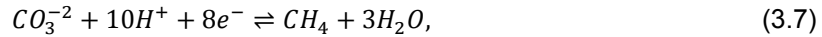
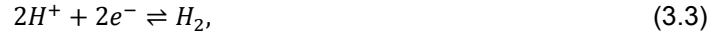
Figure 2.6: Core porosity map

3

Simulation Model

3.1. Aqueous model and reduction to elements

As it is discussed in chapter 1.1.1, there are numerous chemical reactions happening in aqueous phase. In order to capture a calcite dissolution phenomenon with a higher degree of accuracy, an extensive aqueous model is utilized which is described by the following set of chemical reactions:



where reaction 3.6 is required to account for high CO_2 solubility at high pressure and temperature. Altogether with calcite dissolution reactions 1.1, 1.2 and 1.3 we come up with 11 components, which are: H_2O , H^+ , OH^- , CO_2 , HCO_3^- , CO_3^{2-} , $CaCO_3$, Ca^{2+} , $CaOH^+$, $CaHCO_3^+$ and $CaCO_{3,solid}$. As reactions 3.2, 3.3 and 3.7 are very unlikely to occur at the given conditions, components CH_4 and e^- are not considered for simplicity, even though they can be effortlessly included. With such definition there must be 11 equations to solve. To decrease the complexity, we reduce components to elements using equation 1.27. For that purpose we first construct stoichiometry and rate annihilation matrices [35].

For stoichiometry matrix we consider reactions 3.1, 3.4, 3.5, 3.8, 3.9 and 3.10 which are treated as equilibrium reactions and kinetic calcite dissolution:



Hence, stoichiometry matrix is:

$$\mathbf{S} = \begin{matrix} & q_1 & q_2 & q_3 & q_4 & q_5 & q_6 & k_1 \\ \begin{matrix} H_2O \\ H^+ \\ OH^- \\ CO_2 \\ HCO_3^- \\ CO_3^{2-} \\ CaCO_3 \\ Ca^{2+} \\ CaOH^+ \\ CaHCO_3^+ \\ CaCO_{3,solid} \end{matrix} & \begin{bmatrix} -1 & 0 & 1 & -1 & 0 & 0 & 0 \\ 1 & -1 & -2 & 1 & 0 & -1 & 0 \\ 1 & 0 & 0 & 0 & 0 & 0 & 0 \\ 0 & 0 & 1 & 0 & 0 & 0 & 0 \\ 0 & 1 & 0 & 0 & 0 & 0 & 0 \\ 0 & -1 & -1 & 0 & -1 & -1 & 1 \\ 0 & 0 & 0 & 0 & 1 & 0 & 0 \\ 0 & 0 & 0 & -1 & -1 & -1 & 1 \\ 0 & 0 & 0 & 1 & 0 & 0 & 0 \\ 0 & 0 & 0 & 0 & 0 & 1 & 0 \\ 0 & 0 & 0 & 0 & 0 & 0 & -1 \end{bmatrix} \end{matrix} \quad (3.12)$$

In this study we define our elements as H, O, C, Ca and $CaCO_{3,solid}$. Therefore, rate annihilation matrix becomes:

$$\mathbf{E} = \begin{matrix} & H_2O & H^+ & OH^- & CO_2 & HCO_3^- & CO_3^{2-} & \dots & CaCO_{3,solid} \\ \begin{matrix} H \\ O \\ C \\ Ca \\ CaCO_{3,solid} \end{matrix} & \begin{bmatrix} 2 & 1 & 1 & 0 & 1 & 0 & \dots & 0 \\ 1 & 0 & 1 & 2 & 3 & 3 & \dots & 3 \\ 0 & 0 & 0 & 1 & 1 & 1 & \dots & 1 \\ 0 & 0 & 0 & 0 & 0 & 0 & \dots & 1 \\ 0 & 0 & 0 & 0 & 0 & 0 & \dots & 1 \end{bmatrix} \end{matrix} \quad (3.13)$$

Now that the system is defined in terms of components, we implement equation 1.27. This way, we still satisfy following assumption:

$$\sum_{e=1}^E z_e = 1. \quad (3.14)$$

3.2. PHREEQC modeling

PHREEQC [46] is a computer program written in the C and C++ programming languages that is designed to perform a wide variety of aqueous geochemical calculations. Here we use this tool to perform flash calculations and to convert from elements (H, O, C and Ca) back to components (H_2O , CO_2 , $CaCO_3$ and etc.). Model implemented in PHREEQC takes pressure and temperature along with solution composition as an input. In this approach the conservation equations are solved for elements as for components and no rate annihilation matrix is required due to the PHREEQC capability to uniquely map from elements back to components. Kinetic reaction rate is calculated based on the results of PHREEQC simulation output.

Phase split calculations are implemented by introduction of the element based input to aqueous phase for the reaction. Liquid-vapor phase split is realized by introduction of possible gaseous components to the model and defining their partial pressures as zeros at the initial stage. Using Peng-Robinson EoS with critical parameters for a used components defined in the data base, PHREEQC determines the amount of gaseous components that

should appear in gaseous phase at a given conditions of pressure, temperature and composition. Elements-to-components conversion is allowed due to instantaneous local equilibrium assumption. All equilibrium chemical reactions are defined in the default database (phreeqc.dat). Example of PHREEQC implementation of flash calculations is given in a code snippet below.

```
SOLUTION 1
  temp      50.00
  pressure  99.68
  pH        7 charge
  -water    1 # kg
REACTION 1
  Ca        4
  C         8
  O        20
  1
GAS_PHASE 1
  -fixed_pressure
  -pressure 99.68
  CO2(g)   0.0
  H2O(g)   0.0
END
```

Example case represents the following system composition:

- 55.50622 moles of H₂O, which is one kilogram of water,
- 4 moles of CaCO₃, and
- 4 moles of CO₂.

Such model would provide species distribution in aqueous and gaseous phases, saturation indices, saturation ratios, hydrogen activity and other values that are not of the first importance for our study. With default settings, PHREEQC solves conservation equations with the precision of 1e-8, so all lower values are considered to be zeros. Additional closing assumption is electric neutrality condition which is applied for hydrogen ion.

3.2.1. Thermodynamic and chemical equilibrium

In order to resolve complex phase behavior, PHREEQC rewrites all aqueous species in terms of master species according to PHREEQC definitions. Each master species, as it is defined, associated with a particular element, like Ca⁺ for calcite, or its valence state, as Fe⁺³ for ferric iron. Set of unknowns that PHREEQC must solve for are: the natural log of the activities of master species, the natural log of the activity of water, α_{H_2O} , the ionic strength, μ , and the mass of solvent water in an aqueous solution, W_{aq} . The following relations are applied to all master species, except for electrons and water itself:

$$\alpha_i = \gamma_i m_i, \quad (3.15)$$

$$n_i = m_i W_{aq}, \quad (3.16)$$

where γ_i – activity coefficient of master species i , m_i – molality of species i and n_i – moles of master species i in solution. From the law of mass action, eq.(3.16) is rewritten as:

$$n_i = K_i W_{aq} \frac{\prod_m^{M_{aq}} \alpha_m^{c_{m,i}}}{\gamma_i}, \quad (3.17)$$

where m stands for master species and i stands for species. The derivatives of n_i are resolved by Newton-Raphson method. The total derivative is:

$$dn_i = n_i \left(d \ln(W_{aq}) + \sum_m^{M_{aq}} c_{m,i} d \ln(\alpha_m) - \frac{\partial}{\partial \mu} \ln(\gamma_i) d\mu \right). \quad (3.18)$$

With activities defined by Davies equation:

$$\log \gamma_i = Az_i^2 \left(\frac{\sqrt{\mu}}{1 + \sqrt{\mu}} - 0.3\mu \right), \quad (3.19)$$

and by extended or Debye-Hückel equation:

$$\log \gamma_i = -\frac{Az_i^2 \sqrt{\mu}}{1 + B\alpha_i^0 \sqrt{\mu}}, \quad (3.20)$$

their derivatives are

$$\frac{\partial}{\partial \mu} \ln \gamma_i = -\ln(10) \left(Az_i^2 \left(\frac{1}{2\sqrt{\mu}(\sqrt{\mu} + 1)^2} - 0.3 \right) \right), \quad (3.21)$$

and

$$\frac{\partial}{\partial \mu} \ln \gamma_i = -\ln(10) \left(\frac{Az_i^2}{2\sqrt{\mu}(B\alpha_i^0 \sqrt{\mu} + 1)^2} \right). \quad (3.22)$$

Here A and B – temperature dependent constants, z_i – the ionic charge of aqueous species i and α_i^0 – the ion-size parameter. In general, Davies equation is used for charged species and Debye-Hückel equation is used for uncharged species.

Regarding phase split, PHREEQC manual from 1999 [47] states that ideal gases are assumed and gas fugacity is simply equal to its partial pressures. However, newer sources usually state that gas pressures and fugacity coefficients are calculated with Peng-Robinson's EoS [16]. However, every time in the presence of gaseous phase, there is one additional unknowns for PHREEQC to solve, which is total moles of gas components in gaseous phase. Nevertheless, we refer to [47] for a full description of all assumptions, formulas and numerical approaches applied.

3.2.2. PHREEQC – DARTS coupling

PHREEQC is compatible with scripting languages like R and Python [10]. Since DARTS is implemented as C++ engine wrapped by Python interface, PHREEQC – DARTS coupling is easy to achieve. Using Python package to interact with Windows COM framework, PHREEQC is initialized as an callable object before simulation and used later when necessary.

3.3. Kinetic reaction rate

Kinetic reaction rate from [45] is implemented in DARTS framework:

$$r_k = SA \cdot n_0 \cdot t \cdot (KT_a + KT_n) \cdot (1 - SR), \quad (3.23)$$

where SA – reactive surface area, n_0 – initial amount of calcite in moles and SR – calcite saturation ratio. Multipliers t, KT_a and KT_n are defined as follows:

$$t = \left(\frac{n_c}{n_0} \right)^n, \quad (3.24)$$

$$KT_a = k_{25,a} \cdot \exp\left(\frac{-E_a}{R} \cdot \left(\frac{1}{T} - \frac{1}{298.15}\right)\right) \cdot \alpha_{H^+}^{n_a}, \quad (3.25)$$

$$KT_n = k_{25,n} \cdot \exp\left(\frac{-E_n}{R} \cdot \left(\frac{1}{T} - \frac{1}{298.15}\right)\right), \quad (3.26)$$

where n_c – current amount of calcite in moles, n – reaction factor (2/3 for sphere dissolution), $k_{25,a}$ and $k_{25,n}$ – rate constant at 25 °C and pH = 0 for acidic and neutral dissolution mechanisms respectively, E_a and E_n – Arrhenius activation energy for acidic and neutral dissolution mechanisms respectively, R – gas constant, T – temperature in Kelvin and α_{H^+} – activity of hydrogen ion. According to eq.(1.37), γ operator is multiplied by control volume, therefore rate expression is divided by volume. We also neglect t term (reactive surface correction). Eq.(3.23) adapted for implementation in DARTS becomes:

$$r_k = SA \cdot S_{solid} \cdot (1 + c_r \cdot (p - p_{ref}) \cdot \rho) \cdot (KT_a + KT_n) \cdot (1 - SR) \cdot \frac{1}{M_{CaCO_3}} \quad (3.27)$$

where S_{solid} – saturation of solid phase, c_r – calcite compressibility, ρ – calcite density and M_{CaCO_3} – calcite molar mass.

The matrix multiplication of **E** and **S** matrices defines a stoichiometry vectors v for all reactions in terms of elements as a columns of resulting matrix:

$$\mathbf{E} \cdot \mathbf{S} = \begin{matrix} & & q_1 & q_2 & q_3 & q_4 & q_5 & q_6 & k_1 \\ H & & 0 & 0 & 0 & 0 & 0 & 0 & 0 \\ O & & 0 & 0 & 0 & 0 & 0 & 0 & 3 \\ C & & 0 & 0 & 0 & 0 & 0 & 0 & 1 \\ Ca & & 0 & 0 & 0 & 0 & 0 & 0 & 1 \\ CaCO_{3,solid} & & 0 & 0 & 0 & 0 & 0 & 0 & -1 \end{matrix} \quad (3.28)$$

3.4. Permeability treatment

To adequately model wormhole phenomenon we also account for transmissibility change with dissolution. Since molar compositional formulation is implemented, solid phase is included in overall composition as immovable phase and total porosity is 1, the maximum permeability is evaluated by the following power law:

$$K = 1.25^4 \phi^4. \quad (3.29)$$

Here ϕ is assumed to be the total porosity (in this case just 1). This permeability is used for maximum interface transmissibility, T^{max} , initialization and later corrected with respect to the actual value of a fluid porosity (ϕ^f).

$$T(\phi^{n+1}) = T^{max} \cdot T^m(\phi^{n+1}), \quad (3.30)$$

where

$$\phi^{n+1} = \frac{\phi_i^{n+1} + \phi_j^{n+1}}{2}, \quad (3.31)$$

and m is so-called transmissibility multiplier that is used as a fitting parameter.

3.5. Model initialization

Model composition must be defined in terms of molar fraction. However, solid composition is defined as saturation, meaning the conversion from saturation to mole fraction is required.

For this purpose, it is necessary to perform flash calculations for each control volume in order to estimate the densities of the phases at the given conditions. In reality, this type of calculations is very expensive and dramatically increase the initialization time. Therefore, it was decided to develop a simple framework using DARTS capabilities.

The idea of quick model initialization is quite straightforward and can be described with the flowchart in figure 3.1. The same scheme is implemented to convert from composition to saturation at the end of the simulation to avoid very slow results interpretation.

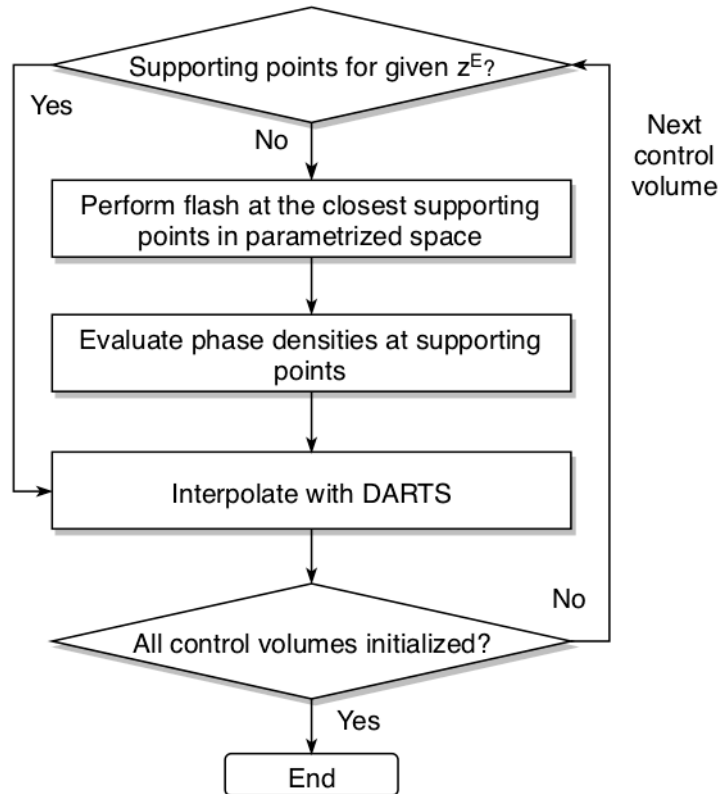


Figure 3.1: Initialization flowchart

Supporting point is an OBL concept and can be interpreted as a point in parameter space that is located at a certain distance from the actual system state. There are as many points as 2^{x-1} , where x is the number of elements in \mathbf{z}^E .

4

Reactive Transport Simulation Results

In this chapter we demonstrate the results of the numerical experiment and compare it to the experimental study. Table 4.1 describes the computer configuration that the model is run on. Developed model doesn't implement any multi-thread routines.

Table 4.1: Computer configuration

<i>Model</i>	
CPU	i7-4850HQ
RAM	16 GB
OS	Windows 10 Pro V1903

4.1. Reactive transport in 1D

Table 4.2 shows the common set of parameters used for a 1D simulation runs. Results

Table 4.2: 1D model configuration

<i>Parameter</i>	<i>Value</i>	<i>Units</i>
Number of blocks	100	[-]
Spatial resolution	1	mm
OBL resolution	201	[-]
Porosity	0.3	[-]
Temperature	50	C°
Initial pressure	100	bar
Production BHP	100	bar
Water : CO ₂ ratio	11:1	[-]

given in figure 4.1 are obtained for a various injection rates. Injection rate variation changes Damköhler and Péclet numbers, which are the main characteristics of dissolution regime. Indeed, lower injection rate results in more stable dissolution front. Higher injection rates result in more amounts of acid penetrating deeper into the domain making a dissolution front less sharp.

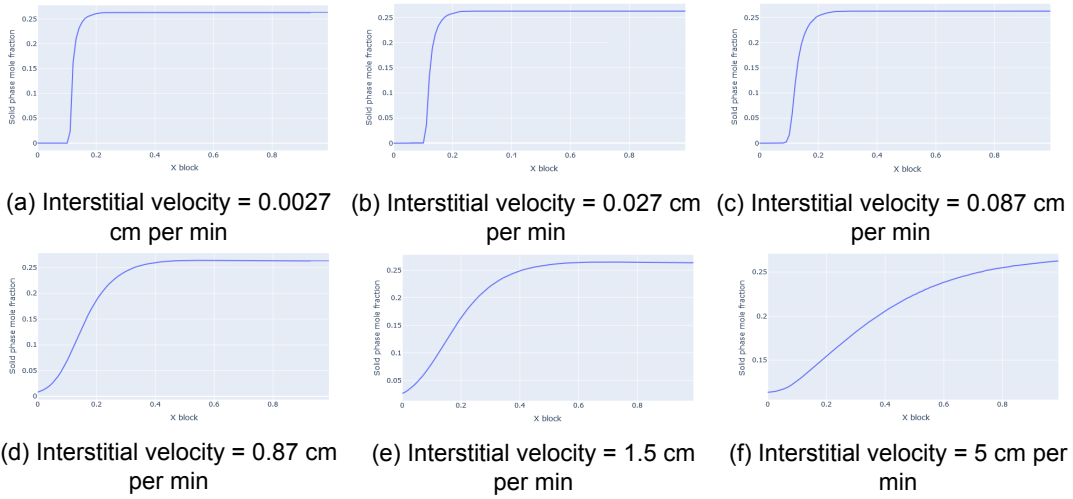


Figure 4.1: Resulting solid saturation in 1D after 10 pore volumes injected

4.2. Reactive transport in 2D

For two dimensional single flow simulation we define a domain with the following parameters listed in table 4.3. Heterogeneous porosity is defined randomly as:

$$\phi(rand) = \begin{cases} 0.263 & 100 \leq rand \leq 80, \\ 0.270 & 80 \leq rand \leq 60, \\ 0.278 & 60 \leq rand \leq 40, \\ 0.286 & 40 \leq rand \leq 20, \\ 0.293 & 20 \leq rand \leq 0, \end{cases} \quad (4.1)$$

where rand is a random number within a range [0, 100]. Such definition doesn't assume any spatial correlation. Initial porosity is given in figure 4.2. Spatial resolution is chosen to

Table 4.3: 2D model configuration

<i>Parameter</i>	<i>Value</i>	<i>Units</i>
Number of blocks	75-by-75-by-1	[-]
Spatial resolution	1 × 1 × 60	mm
OBL resolution	201	[-]
Temperature	50	C°
Initial pressure	100	bar
Production BHP	100	bar
Injection rate	1.1	ml per min
Diffusion coefficient	4.5e-5	m ² per day
Water : CO ₂ ratio	11:1	[-]
Simulation time	27	hours

satisfy experimental interstitial velocity, which is calculated as:

$$u_i = \frac{u_s}{\phi}, \quad (4.2)$$

$$u_s = \frac{Q}{A}, \quad (4.3)$$

where u_s – superficial velocity, Q – volumetric injection rate and A – cross-section area, which is calculated according to the core diameter used in the experiment. Therefore, with the core

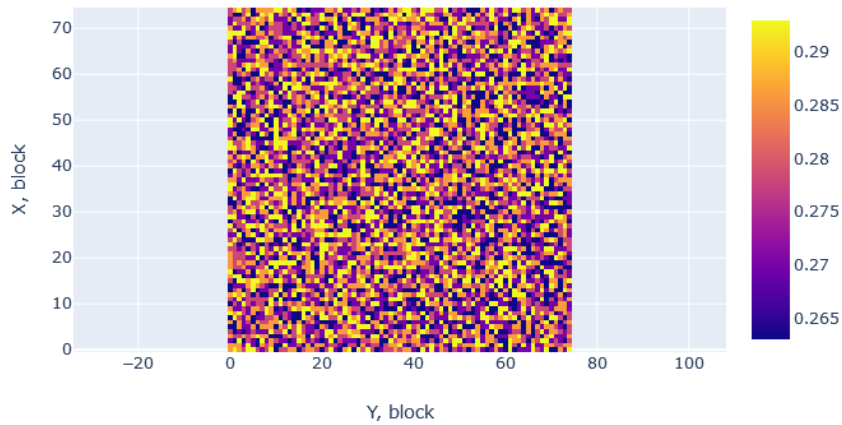


Figure 4.2: Initial porosity distribution in 2D

diameter of 7.5 cm, volumetric injection rate of 1.1 ml per minute and mean porosity of 0.278 the interstitial velocity constitutes 0.0896 cm per minute. Corresponding cross-section area per block in 2D model is evaluated to be 58.9 mm, hence, 60 mm is assumed.

Resulting porosity distribution after a 27 hours of injection at a constant temperature, production pressure and injection rate are given in the figure 4.3 along with solid phase molar fraction and numerical results present in [54]. Simulation run performance parameters are

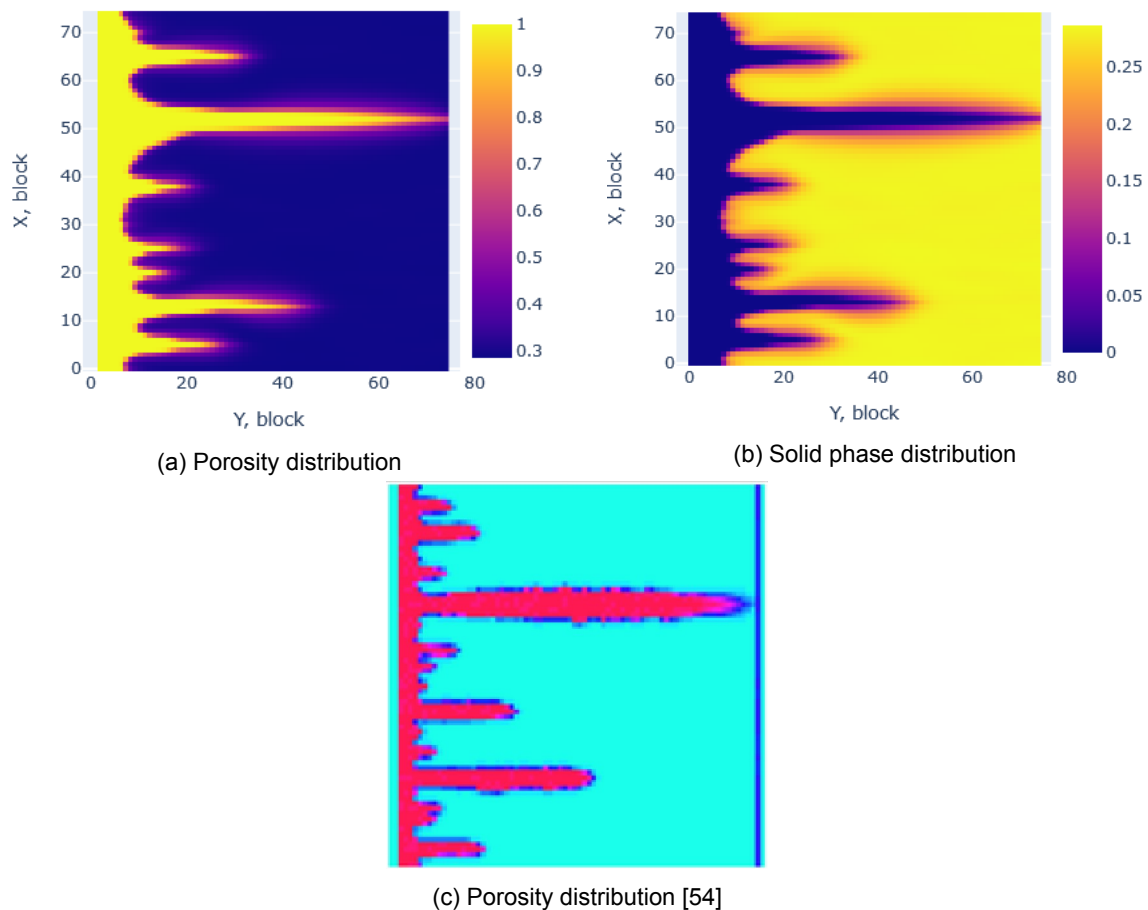


Figure 4.3: 2D simulation results

depicted in table 4.4.

Table 4.4: 2D simulation performance

<i>Parameter</i>	<i>Value</i>	<i>Units</i>
Run time	135.027	s
Time steps	195	[-]
Total iterations (Newton)	623	[-]

Qualitative comparison shows reasonable match in terms of break-through time and competing wormholes spatial distribution. One noticeable mismatch is observed at the injection region where numerical results show stable dissolution front, which is not present in the original experimental results (figure 4.5). Nevertheless, obtained results are in good agreement with the numerical solution from [54] with minor deviation, like main and competing wormholes propagation distance. It can be caused by model sensitivity to OBL resolution setting. Additionally, pressure drop in the beginning and the end of simulation (figure 4.4) aligns well with the the reported values.

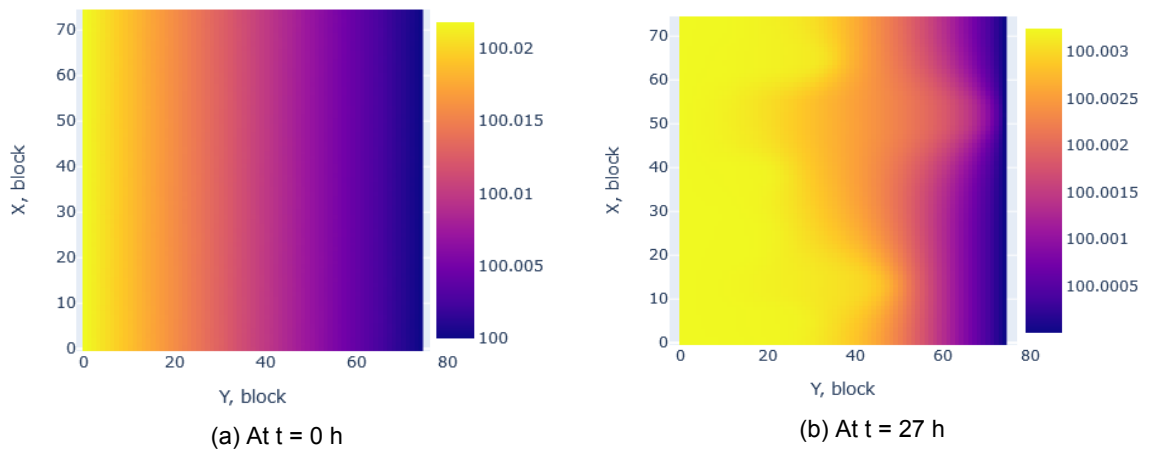


Figure 4.4: 2D model pressure drop (bar)

Utilizing one of the OBL features, we also measured the model performance with pre-computed OBL points, i.e. repeated simulation run with the same definition of physics and chemistry (table 4.5). Difference in run time and similarity in the other performance parameters indirectly indicate time spend for physics computations.

Table 4.5: 2D simulation performance

<i>Parameter</i>	<i>Value</i>	<i>Units</i>
Run time	51.567	s
Time steps	195	[-]
Total iterations (Newton)	623	[-]

4.3. Reactive transport in 3D

In this section we introduce the simulation results in 3D domain that is reconstructed from the CT data. Model configuration is given in table 4.6. The resulting solid phase molar fraction is depicted in figure 4.5 together with the interpreted experimental CT. There is a significant mismatch between the actual and numerical experiment in terms of wormhole

Table 4.6: 3D model configuration

<i>Parameter</i>	<i>Value</i>	<i>Units</i>
Total number of blocks	185008	[-]
OBL resolution	201	[-]
Temperature	50	C°
Initial pressure	100	bar
Production BHP	100	bar
Injection rate	1.1	ml per min
Diffusion coefficient	4.5e-5	m ² per day
Water : CO ₂ ratio	11:1	[-]
Simulation time	27	hours

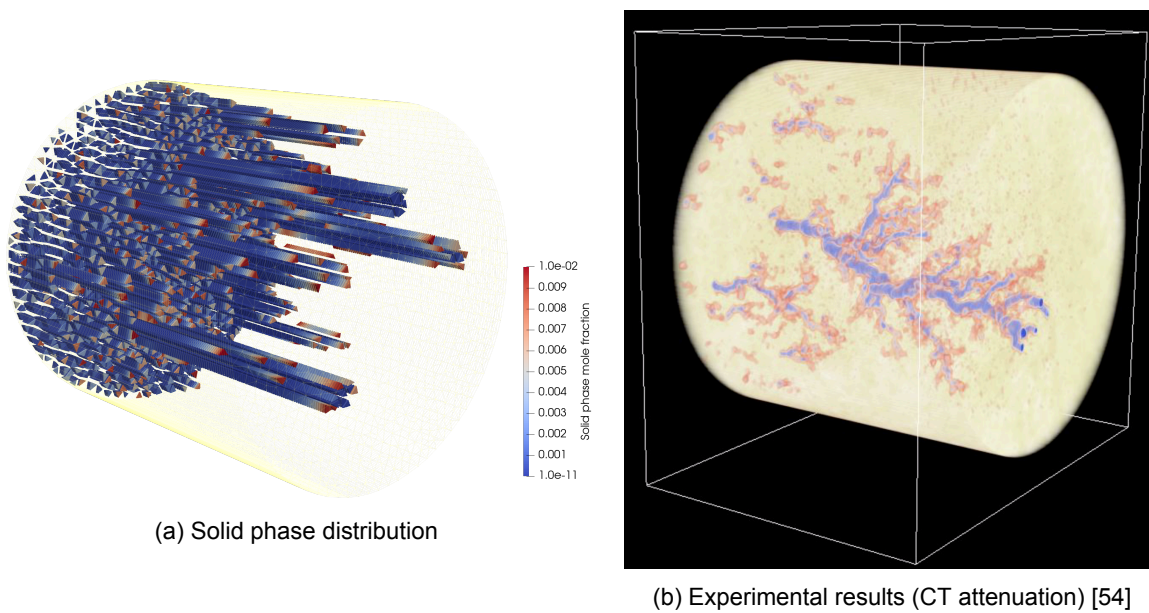


Figure 4.5: Solid phase molar fraction

trajectory. Observed discrepancy is expected due to the mesh structure described in chapter 2.3. Insufficiently high spatial resolution may also contribute to the observed deviation between the actual experiment and numerical simulation. Nevertheless, breakthrough time is the same as reported from experimental study, therefore constructed model predicts the main feature of interest for at least this particular setting. Simulation run performance parameters are depicted in table 4.7.

Table 4.7: 3D simulation performance

<i>Parameter</i>	<i>Value</i>	<i>Units</i>
Run time	53317.765	s
Time steps	393	[-]
Total iterations (Newton)	941	[-]

5

Conclusion and Recommendations for Future Work

Due to high degree of nonlinearity we were unable to run the simulation for a timestep higher than 0.02 day. Appleyard chop technique may be a good solution when applied to kinetic reaction rate and prevent PHREEQC from crashing due to large composition values update. Once implemented, developed solver can be tested at bigger systems with higher time step and run time. Another enhancement that can possibly be done to the developed solution is the implementation of upscaling techniques to correlate core scale solution with the reservoir scale models in order to preserve DARTS performance and capture wormholing phenomenon in large systems. In this study, we were focused on a single phase experiment, however the model was developed with the possible extension to multiphase physics in mind. Besides multiphase flow, DBS equation for flow instead of Darcy equation is a reasonable improvement, at least for the research purposes, as DBS usually shows different propagation speed of a dissolution front.

Regarding homogeneous dissolution at the near-to-injection area, this phenomenon is not yet well understood. There are various parameters that could possibly cause such result, like experimental setting, fine details of which were not considered for the numerical solution, or little adjustments to CT data for better visual representation of wormholes. More accurate modeling of the injection may result in lower times for instabilities to cause wormholes to appear. In fact, inlet and outlet effects may deserve a dedicated study.

We consider current simulation output as a preliminary result, therefore, sensitivity study is a logical continuation or, at least, extension for this project. In particular, better understanding of spatial and OBL resolutions on the final results would provide a deeper understanding of the solver capabilities allowing for more robust and fast models in future applications. Alongside sensitivity to the resolution setting the permeability change estimation check may provide valuable insights on the wormholing process in general. More accurate treatment of changing block transmissibilities can potentially enhance solver ability to capture wormholes' shape, propagation speed and spatial distribution with higher degree of accuracy. This improvement, however, is rather related to pore scale area of studies.

There is a room for improvements in an image processing area as well. One of the drawbacks in this section is the 3D mesh structure. Even though mesh is unstructured as shown in chapter 2.3, it is structured in the direction of the flow. Such decision is made because of flow direction and also due to the complications related to property calculations for the fully unstructured grid. One of our suggestions would be to populate CT information by imple-

mentation of machine learning (ML) algorithms in order to predict a numerical value of the CT attenuation between the adjacent slices. One of the applicable solutions is Generative Adversarial Network (GAN). The idea here is to train a model to predict pixel values using for slice n using slices $n - 1$ and $n + 1$ and then predict new images between slices $n - 1$ and n . Of course, resulting images must be validated since such model may not capture the nature of a rock sample properly because of the varying distance between slices.

Another idea would be to use k-nearest neighbours (KNN) and some regression algorithm to predict pixel values. If all pixel values could be classified into several well pronounced groups, the pixel values of missing slices could be predicted by the class of the pixels on bounding slices and their values.

Such data can be used to optimize the population approach and obtain an important insight regarding CT processing with ML. Although this technique doesn't replace a real images, it potentially might provide additional data for more detailed modeling of a core. As an alternative it is also possible to use less sophisticated techniques. One of our considerations was to evaluate the control volume porosity based on weighted average of the nearest 2D ROI's to the control volume center, where weights are the distances. In essence, it is very close to KNN algorithm.

Bibliography

- [1] Gabor Acs, Sandor Doleschall, and Eva Farkas. General purpose compositional model. *Society of Petroleum Engineers Journal*, 25(04):543–553, aug 1985. doi: 10.2118/10515-pa.
- [2] F. M. Auzerais, J. Dunsmuir, B. B Ferréol, N. Martys, J. Olson, T. S. Ramakrishnan, D. H. Rothman, and L. M. Schwartz. Transport in sandstone: A study based on three dimensional microtomography. *Geophysical Research Letters*, 23(7):705–708, apr 1996. doi: 10.1029/96gl00776.
- [3] L. A. Barrios, J. E. Quijano, R. E. Romero, H. Mayorga, M. Castro, and J. Caldera. Enhanced permeability by chemical stimulation at the berlin geothermal field, el salvador. *Geothermal Resources Council Transactions*, 26, 2002. ISSN 0193-5933.
- [4] D.A. Barry, C.T. Miller, P.J. Culligan, and K. Bajracharya. Analysis of split operator methods for nonlinear and multispecies groundwater chemical transport models. *Mathematics and Computers in Simulation*, 43(3-6):331–341, mar 1997. doi: 10.1016/s0378-4754(97)00017-7.
- [5] Martin J. Blunt, Branko Bijeljic, Hu Dong, Oussama Gharbi, Stefan Iglauer, Peyman Mostaghimi, Adriana Paluszny, and Christopher Pentland. Pore-scale imaging and modelling. *Advances in Water Resources*, 51:197–216, jan 2013. doi: 10.1016/j.advwatres.2012.03.003.
- [6] G. Bradski. The OpenCV Library. *Dr. Dobb’s Journal of Software Tools*, 2000.
- [7] Marten Adriaan Buijse and Gerard Glasbergen. A semi-empirical model to calculate wormhole growth in carbonate acidizing. In *SPE Annual Technical Conference and Exhibition*. Society of Petroleum Engineers, 2005. doi: 10.2118/96892-ms.
- [8] Jérôme Carrayrou, Robert Mosé, and Philippe Behra. Operator-splitting procedures for reactive transport and comparison of mass balance errors. *Journal of Contaminant Hydrology*, 68(3-4):239–268, feb 2004. doi: 10.1016/s0169-7722(03)00141-4.
- [9] Frank Chang, Qi Qu, and Wayne Frenier. A novel self-diverting-acid developed for matrix stimulation of carbonate reservoirs. In *SPE International Symposium on Oilfield Chemistry*. Society of Petroleum Engineers, 2001. doi: 10.2118/65033-ms.
- [10] S. R. Charlton and D. L. Parkhurst. Modules based on the geochemical model phreeqc for use in scripting and programming languages. *Computers & Geosciences*, 37:1653–1663, 2011. URL <http://dx.doi.org/10.1016/j.cageo.2011.02.005>.
- [11] M.C.H. Chien, S.T. Lee, and W.H. Chen. A new fully implicit compositional simulator. In *SPE Reservoir Simulation Symposium*. Society of Petroleum Engineers, 1985. doi: 10.2118/13385-ms.
- [12] Lei Chou, Robert M. Garrels, and Roland Wollast. Comparative study of the kinetics and mechanisms of dissolution of carbonate minerals. *Chemical Geology*, 78(3-4):269–282, dec 1989. doi: 10.1016/0009-2541(89)90063-6.
- [13] Robert Cimrman, Vladimír Lukeš, and Eduard Rohan. Multiscale finite element calculations in python using sfepy. *Advances in Computational Mathematics*, 2019. ISSN 1572-9044. doi: 10.1007/s10444-019-09666-0. URL <https://doi.org/10.1007/s10444-019-09666-0>.

- [14] Keith H. Coats. An equation of state compositional model. *Society of Petroleum Engineers Journal*, 20(05):363–376, oct 1980. doi: 10.2118/8284-pa.
- [15] *GEM user guide*. Computer Modeling Group, 2014.
- [16] P.J. de Moel, J.C. van Dijk, and W.G.J. van der Meer. Aquatic chemistry for engineers, self study course on phreeqc for modelling water quality and water treatment, November 2013.
- [17] Hang Deng, Jeffrey P. Fitts, and Catherine A. Peters. Quantifying fracture geometry with x-ray tomography: Technique of iterative local thresholding (TILT) for 3d image segmentation. *Computational Geosciences*, 20(1):231–244, feb 2016. doi: 10.1007/s10596-016-9560-9.
- [18] Jean E. Elkhoury, Raji Shankar, and T. S. Ramakrishnan. Resolution and limitations of x-ray micro-CT with applications to sandstones and limestones. *Transport in Porous Media*, 129(1):413–425, apr 2019. doi: 10.1007/s11242-019-01275-1.
- [19] Peter Engesgaard and Kenneth L. Kipp. A geochemical transport model for redox-controlled movement of mineral fronts in groundwater flow systems: A case of nitrate removal by oxidation of pyrite. *Water Resources Research*, 28(10):2829–2843, oct 1992. doi: 10.1029/92wr01264.
- [20] B. Bazin R. Lenormand D. Lasseux F. Golfier, C. Zarcone and M. Quintard. On the ability of a darcy-scale model to capture wormhole formation during the dissolution of a porous medium. *Journal of Fluid Mechanics*, 457, apr 2002. doi: 10.1017/s0022112002007735.
- [21] Marwan Fahs, Jérôme Carrayrou, Anis Younes, and Philippe Ackerer. On the efficiency of the direct substitution approach for reactive transport problems in porous media. *Water, Air, and Soil Pollution*, 193(1-4):299–308, apr 2008. doi: 10.1007/s11270-008-9691-2.
- [22] Yaqing Fan. *Chemical Reaction Modeling in a Subsurface Flow Simulator with Application to in-situ Upgrading and CO2 Mineralization*. PhD thesis, Stanford University, 2010.
- [23] Sara Forough Farshidi. *Compositional Reservoir Simulation-based Reactive-transport Formulations, with Application to CO2 Storage in Sandstone and Ultramafic Formations*. PhD thesis, Stanford University, April 2016.
- [24] Tiago Ferreira and Wayne Rasband. *ImageJ User Guide IJ 1.46r. Revised edition*, October 2012.
- [25] C.N. Fredd and H.S. Fogler. Optimum conditions for wormhole formation in carbonate porous media: Influence of transport and reaction. *SPE Journal*, 4(03):196–205, sep 1999. doi: 10.2118/56995-pa.
- [26] C.N. Fredd and M.J. Miller. Validation of carbonate matrix stimulation models. In *SPE International Symposium on Formation Damage Control*. Society of Petroleum Engineers, 2000. doi: 10.2118/58713-ms.
- [27] Christophe Geuzaine and Jean-François Remacle. Gmsh: A 3-d finite element mesh generator with built-in pre- and post-processing facilities. *International Journal for Numerical Methods in Engineering*, 79(11):1309–1331, sep 2009. doi: 10.1002/nme.2579.
- [28] Kenneth M. Hanson. Noise and computed contrast discrimination in tomography. In *Radiology of the Skull and Brain, Vol. 5: Technical Aspects of Computed Tomography*, chapter 113. St Louis : C V Mosby Co, 1981.
- [29] A. Daniel Hill and Robert S. Schechter. Fundamentals of acid stimulation. In *Reservoir Stimulation, 3rd Edition*, chapter 16. Wiley, 2000. ISBN 0471491926.

- [30] David L. Hochstetler, Massimo Rolle, Gabriele Chiogna, Christina M. Haberer, Peter Grathwohl, and Peter K. Kitanidis. Effects of compound-specific transverse mixing on steady-state reactive plumes: Insights from pore-scale simulations and darcy-scale experiments. *Advances in Water Resources*, 54:1–10, apr 2013. doi: 10.1016/j.advwatres.2012.12.007.
- [31] M. L. Hoefner and H. S. Fogler. Pore evolution and channel formation during flow and reaction in porous media. *AIChE Journal*, 34(1):45–54, jan 1988. doi: 10.1002/aic.690340107.
- [32] J. Guillermo Jaimes-Maldonado and Raul Sanchez-Velasco. Acid stimulation of production wells in las tres virgenes geothermal field, bcs, mexico. *Geothermal Resources Council Transactions*, 27, 2003. ISSN 0193-5933.
- [33] V. Joekar-Niasar, M. I. J. van Dijke, and S. M. Hassanizadeh. Pore-scale modeling of multiphase flow and transport: Achievements and perspectives. *Transport in Porous Media*, 94(2):461–464, jul 2012. doi: 10.1007/s11242-012-0047-4.
- [34] Keshav Kala. Parameterization of element balance formulation in reactive compositional flow and transport. Master’s thesis, Delft University of Technology, 2017.
- [35] Keshav Kala and Denis Voskov. Element balance formulation in reactive compositional flow and transport with parameterization technique. *Computational Geosciences*, Jun 2019. ISSN 1573-1499. doi: 10.1007/s10596-019-9828-y.
- [36] Mark Khait and Denis V. Voskov. Operator-based linearization for general purpose reservoir simulation. *Journal of Petroleum Science and Engineering*, 157:990–998, aug 2017. doi: 10.1016/j.petrol.2017.08.009.
- [37] Michael Krause, Jean-Christophe Perrin, Chia-Wei Kuo, and Sally M. Benson. Characterization of CO₂ storage properties using core analysis techniques and thin section data. *Energy Procedia*, 1(1):2969–2974, feb 2009. doi: 10.1016/j.egypro.2009.02.073.
- [38] Li Li, Carl I. Steefel, and Li Yang. Scale dependence of mineral dissolution rates within single pores and fractures. *Geochimica et Cosmochimica Acta*, 72(2):360–377, jan 2008. doi: 10.1016/j.gca.2007.10.027.
- [39] Peter C. Lichtner. Continuum model for simultaneous chemical reactions and mass transport in hydrothermal systems. *Geochimica et Cosmochimica Acta*, 49(3):779 – 800, 1985. ISSN 0016-7037.
- [40] Peter C. Lichtner, Glenn E. Hammond, Chuan Lu, Satish Karra, Gautam Bisht, Benjamin Andre, Richard T. Mills, Jitendra Kumar, and Jennifer M. Frederick. *PFLOTRAN User Manual*, 2019. <http://documentation.pflotran.org>.
- [41] Xinghui Liu, Anne Ormond, Kirk Bartko, Li Ying, and Peter Ortoleva. A geochemical reaction-transport simulator for matrix acidizing analysis and design. *Journal of Petroleum Science and Engineering*, 17(1-2):181–196, feb 1997. doi: 10.1016/S0920-4105(96)00064-2.
- [42] Ayaz Mehmani and Maša Prodanović. The effect of microporosity on transport properties in porous media. *Advances in Water Resources*, 63:104–119, jan 2014. doi: 10.1016/j.advwatres.2013.10.009.
- [43] Sergi Molins, David Trebotich, Carl I. Steefel, and Chaopeng Shen. An investigation of the effect of pore scale flow on average geochemical reaction rates using direct numerical simulation. *Water Resources Research*, 48(3), mar 2012. doi: 10.1029/2011wr011404.
- [44] M. Oostrom, Y. Mehmani, P. Romero-Gomez, Y. Tang, H. Liu, H. Yoon, Q. Kang, V. Joekar-Niasar, M. T. Balhoff, T. Dewers, G. D. Tartakovsky, E. A. Leist, N. J. Hess, W. A. Perkins, C. L. Rakowski, M. C. Richmond, J. A. Serkowski, C. J. Werth, A. J.

- Valocchi, T. W. Wietsma, and C. Zhang. Pore-scale and continuum simulations of solute transport micromodel benchmark experiments. *Computational Geosciences*, 20(4): 857–879, jun 2014. doi: 10.1007/s10596-014-9424-0.
- [45] James Palandri and Yousif Kharaka. A compilation of rate parameters of water-mineral interaction kinetics for application to geochemical modeling. Technical report, U.S. Geological Survey, 03 2004.
- [46] D. L. Parkhurst and C. A. J. Appelo. *Description of input and examples for PHREEQC version 3—A computer program for speciation, batch-reaction, one-dimensional transport, and inverse geochemical calculations*, 2013. URL <http://pubs.usgs.gov/tm/06/a43>.
- [47] David L. Parkhurst and C.A.J. Appelo. *USER'S GUIDE TO PHREEQC (VERSION 2)*, 1999.
- [48] L.Niel Plummer and T.M.L Wigley. The dissolution of calcite in CO₂-saturated solutions at 25°C and 1 atmosphere total pressure. *Geochimica et Cosmochimica Acta*, 40(2):191–202, feb 1976. doi: 10.1016/0016-7037(76)90176-9.
- [49] Bruce A. Robinson, Hari S. Viswanathan, and Albert J. Valocchi. Efficient numerical techniques for modeling multicomponent ground-water transport based upon simultaneous solution of strongly coupled subsets of chemical components. *Advances in Water Resources*, 23(4):307–324, jan 2000. doi: 10.1016/s0309-1708(99)00034-2.
- [50] Maarten W. Saaltink, Jesús Carrera, and Carlos Ayora. On the behavior of approaches to simulate reactive transport. *Journal of Contaminant Hydrology*, 48(3-4):213–235, apr 2001. doi: 10.1016/s0169-7722(00)00172-8.
- [51] Rahman Shaik. Modelling of near-well acidisation. Master's thesis, Delft University of Technology, 2017.
- [52] B.C. Sharma, W.E. Brigham, and L.M. Castanier. CT imaging techniques for two-phase and three-phase in-situ saturation measurements. Technical report, Prepared for U.S. Department of Energy, jun 1997.
- [53] J. Snippe, S. Berg, K. Ganga, and N. Brussee. Experimental and numerical investigation of wormholing during CO₂ storage and water alternating gas injection. In *Computational Methods in Water Resources conference*, 2018.
- [54] Jeroen Snippe, Steffen Berg, Keschma Ganga, Niels Brussee, and Rick Gdanski. Experimental and numerical investigation of wormholing during CO₂ storage and water alternating gas injection. *International Journal of Greenhouse Gas Control*.
- [55] Jeroen Snippe, Rick Gdanski, and Holger Ott. Multiphase modelling of wormhole formation in carbonates by the injection of CO₂. *Energy Procedia*, 114:2972–2984, jul 2017. doi: 10.1016/j.egypro.2017.03.1426.
- [56] Cyprien Soullaine. Mineral dissolution and wormholing from a pore-scale perspective. *Journal of Fluid Mechanics*, 827:457–483, 2017. doi: 10.13140/rg.2.2.35678.43848.
- [57] Cyprien Soullaine, Sophie Roman, Anthony Kavscek, and Hamdi A. Tchelepi. Pore-scale modelling of multiphase reactive flow: application to mineral dissolution with production of. *Journal of Fluid Mechanics*, 855:616–645, sep 2018. doi: 10.1017/jfm.2018.655.
- [58] C. I. Steefel, S. Molins, and D. Trebotich. Pore scale processes associated with subsurface CO₂ injection and sequestration. *Reviews in Mineralogy and Geochemistry*, 77(1): 259–303, jan 2013. doi: 10.2138/rmg.2013.77.8.
- [59] C. I. Steefel, C. A. J. Appelo, B. Arora, D. Jacques, T. Kalbacher, O. Kolditz, V. Lagneau, P. C. Lichtner, K. U. Mayer, J. C. L. Meeussen, S. Molins, D. Moulton, H. Shao, J. Šimůnek, N. Spycher, S. B. Yabusaki, and G. T. Yeh. Reactive transport codes for subsurface environmental simulation. *Computational Geosciences*, 19(3):445–478, sep 2014. doi: 10.1007/s10596-014-9443-x.

- [60] C.I. Steefel. Crunchflow software for modeling multicomponent reactive flow and transport. user's manual. *Earth Sciences Division. Lawrence Berkeley, National Laboratory, Berkeley*, pages 12–91p, 01 2009.
- [61] P. Szymczak and A. J. C. Ladd. Wormhole formation in dissolving fractures. *Journal of Geophysical Research*, 114(B6), jun 2009. doi: 10.1029/2008jb006122.
- [62] P. Tomin and D. Voskov. Robust and accurate formulation for modeling of acid stimulation. In *ECMOR XVI - 16th European Conference on the Mathematics of Oil Recovery*. EAGE Publications BV, sep 2018. doi: 10.3997/2214-4609.201802120.
- [63] *User's guide for UTCHEM-5.32m a three dimensional chemical flood simulator. Final report, September 30, 1992–December 31, 1995*. The University of Texas, 7 1996.
- [64] Harold J. Vinegar and Scott L. Wellington. Tomographic imaging of three-phase flow experiments. *Review of Scientific Instruments*, 58(1):96–107, jan 1987. doi: 10.1063/1.1139522.
- [65] Pauli Virtanen, Ralf Gommers, Travis E. Oliphant, Matt Haberland, Tyler Reddy, David Cournapeau, Evgeni Burovski, Pearu Peterson, Warren Weckesser, Jonathan Bright, Stéfan J. van der Walt, Matthew Brett, Joshua Wilson, K. Jarrod Millman, Nikolay Mayorov, Andrew R. J. Nelson, Eric Jones, Robert Kern, Eric Larson, CJ Carey, İlhan Polat, Yu Feng, Eric W. Moore, Jake VanderPlas, Denis Laxalde, Josef Perktold, Robert Cimrman, Ian Henriksen, E. A. Quintero, Charles R Harris, Anne M. Archibald, Antônio H. Ribeiro, Fabian Pedregosa, Paul van Mulbregt, and SciPy 1.0 Contributors. SciPy 1.0—Fundamental Algorithms for Scientific Computing in Python. *arXiv e-prints*, art. arXiv:1907.10121, Jul 2019.
- [66] Denis V. Voskov. Operator-based linearization approach for modeling of multiphase multi-component flow in porous media. *Journal of Computational Physics*, 337:275–288, may 2017. doi: 10.1016/j.jcp.2017.02.041.
- [67] Denis V. Voskov and Hamdi A. Tchelepi. Comparison of nonlinear formulations for two-phase multi-component eos based simulation. *Journal of Petroleum Science and Engineering*, 82-83:101 – 111, 2012. ISSN 0920-4105.
- [68] S.L. Wellington and H.J. Vinegar. CT studies of surfactant-induced CO2 mobility control. In *SPE Annual Technical Conference and Exhibition*. Society of Petroleum Engineers, 1985. doi: 10.2118/14393-ms.
- [69] S.L. Wellington and H.J. Vinegar. X-ray computerized tomography. *Journal of Petroleum Technology*, 39(08):885–898, aug 1987. doi: 10.2118/16983-pa.
- [70] Tianfu Xu, Eric Sonnenthal, Nicolas Spycher, and Karsten Pruess. *TOUGHREACT User's Guide: A Simulation Program for Non-isothermal Multiphase Reactive geochemical Transport in Variable Saturated Geologic Media*, may 2004.
- [71] Gour-Tsyh Yeh. A critical evaluation of recent developments of hydrogeochemical transport models of reactive multi-chemical components. *Water Resources Research*, 23: 93–108, 01 1989.
- [72] Gour-Tsyh Yeh and Vijay S. Tripathi. A model for simulating transport of reactive multispecies components: Model development and demonstration. *Water Resources Research*, 27(12):3075–3094, dec 1991. doi: 10.1029/91wr02028.
- [73] A Zifan, P Liatsis, and B E Chapman. The use of the kalman filter in the automated segmentation of EIT lung images. *Physiological Measurement*, 34(6):671–694, may 2013. doi: 10.1088/0967-3334/34/6/671.